Discovery of Novel CXCR2 Inhibitors Using Ligand-Based Pharmacophore Models

Helen Ha,[†] Bikash Debnath,[‡] Srinivas Odde,[†] Tim Bensman,[§,∥] Henry Ho,[§,∥] Paul M. Beringer,[§] and Nouri Neamati*,[‡]

[†]Department of Pharmacology and Pharmaceutical Sciences, University of Southern California School of Pharmacy, 1985 Zonal Avenue, Los Angeles, California 90033, United States

[‡]Department of Medicinal Chemistry, College of Pharmacy, and Translational Oncology Program, University of Michigan, North Campus Research Complex, 2800 Plymouth Road, Ann Arbor, Michigan 48109, United States

[§]Department of Clinical Pharmacy, University of Southern California School of Pharmacy, 1985 Zonal Avenue, Los Angeles, California 90033, United States

ⓢ Supporting Information

ABSTRACT: The chemokine receptor CXCR2 is expressed on various immune cells and is essential for neutrophil recruitment and angiogenesis at sites of acute and chronic inflammation caused by tissue injury or infection. CXCR2 and its ligand, CXCL8, are implicated in a number of inflammation-mediated diseases such as chronic obstructive pulmonary disease, cystic fibrosis, and cancer. Though the development of CXCR2-specific small-molecule inhibitors as anti-inflammatory agents has been pursued by pharmaceutical companies within the past decade, there are currently no clinically approved CXCR2 inhibitors. A pharmacophore model based on previously reported CXCR2 antagonists was developed to screen a database of commercially available compounds. Small-molecule compounds identified from the pharmacophore screening were selected for in vitro screening in a cell-based CXCR2-mediated β-arrestin-2 recruitment assay and further characterized in several cell-based assays and lipopolysaccharide (LPS)-induced lung inflammation studies in mice. CX compounds identified from pharmacophore modeling inhibited cell migration, lung and colon cancer cell proliferation, and colony formation. Mechanistic studies of CX4152 showed that this compound inhibits CXCR2 signaling through downregulation of surface CXCR2. Additionally, CX4152 significantly inhibits CXCL8-mediated neutrophil migration and LPS-induced lung inflammation in mice. Using a CXCR2-inhibitor-based pharmacophore model, we identified a novel set of sulfonamides from a diverse library of small molecules. These compounds inhibit CXCR2/β-arrestin-2 association, cell migration and proliferation, and acute inflammation in mouse models. CX compounds identified from our pharmacophore models are potential leads for further optimization and development as anti-inflammatory and anticancer agents.
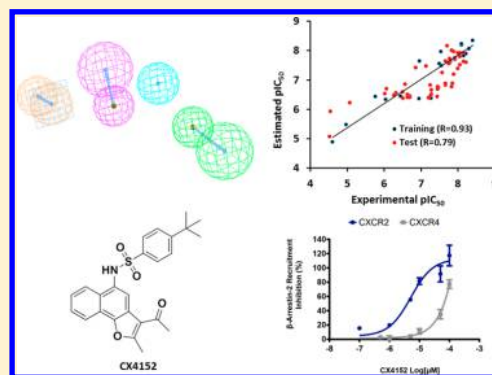
INTRODUCTION

The CXC chemokine receptor 2 (CXCR2) is a G-protein coupled receptor (GPCR) expressed on inflammatory cells such as neutrophils, monocytes, T-lymphocytes, and basophils as well as endothelial cells and central nervous system neurons.[1−5] CXCR2 is activated by several ELR+ chemokines, including interleukin-8 (IL-8 or CXCL8), epithelial-cell-derived neutrophil-activating protein 78 (ENA-78), neutrophil-activating peptide 2 (NAP-2), and Groα.[1,6] The CXCR2 ligand CXCL8 is essential for neutrophil chemotaxis and for angiogenesis during acute and chronic inflammatory conditions caused by tissue injury or infections.[7−10] It also activates CXCR1, another chemokine receptor that is also involved in neutrophil chemotaxis.[1]

Since CXCR2/CXCL8 plays a critical role in inflammation, CXCR2 inhibition may be able to alleviate symptoms of respiratory diseases characterized by neutrophil-mediated inflammation, such as chronic obstructive pulmonary disease (COPD)

and cystic fibrosis (CF). Clinical studies have shown that airway secretions and lung tissue from patients with COPD have increased CXCR2 chemokine ligand levels compared with healthy patients, which negatively correlates with lung function.[11,12] Realizing the anti-inflammatory potential of CXCR2 inhibition, several pharmaceutical companies began to pursue the development of small-molecule CXCR2 inhibitors using high-throughput screening platforms. The first class of CXCR2 inhibitors was discovered in the mid 1990s by GlaxoSmithKline. SB225002 was the first reported CXCR2-selective small-molecule compound, and further developments led to SB265610 and SB656933 (see Table 3).[13,14]

CXCR2 is also expressed by a number of different cancer cells, including lung, colon, ovarian, and prostate cancer cells.[15−18]

CXCL8 derived from tumor-associated macrophages, neutrophils, and tumor cells promotes cancer cell proliferation, survival, invasiveness, tumor angiogenesis, and decreased sensitivity to anticancer agents.[19−21] In addition to CXCL8, other CXCR2 chemokine ligands such as Groα also significantly enhance the proliferation and invasiveness of cancer cells.[22,23] Lung cancer xenograft studies showed that CXCR2 knockout mice have reduced tumor size, reduced spontaneous metastases, and decreased vascular density compared with wild-type mice. In addition, CXCR2^{+/+} mice treated with CXCR2-neutralizing antibodies exhibit phenotypes similar to CXCR2^{−/−} mice.[24] These preclinical studies indicate that CXCR2/CXCL8 is an essential component of the tumor microenvironment that promotes tumor progression, and its inhibition may be therapeutically beneficial for cancer patients. However, currently there are no approved CXCR2 inhibitors, nor are any in clinical trials to assess their efficacy in cancer patients. Given the anti-inflammatory and anticancer therapeutic potential of CXCR2 inhibition, we sought to develop a robust pharmacophore model to identify novel classes of compounds that inhibit CXCR2 function and also show anti-inflammatory and anticancer properties in in vitro and in vivo models.

■ MATERIALS AND METHODS

Molecular Modeling. Molecular modeling was performed on a Dell Precision T7400n Mini-Tower computer with a dual quad-core Xeon X5450 processor with 32 nodes. Catalyst software (version 4.11, Accelrys, San Diego, CA) was used to generate HypoGen pharmacophore models.[25] Molecular docking was performed using the Genetic Optimization for Ligand Docking (GOLD) software package (version 5.2, Cambridge Crystallographic Data Centre (CCDC), Cambridge, U.K.).[26,27] The Rapid Overlay of Chemical Structures (ROCS) software (version 3.2.0.4, OpenEye Scientific Software, Santa Fe, NM) was used to generate shape-based pharmacophore models.[28,29]

Data Set and HypoGen Modeling of the Pharmacophore. Biological activity data (binding assay performed with Chinese hamster ovary (CHO) cell lines expressing CXCR2), represented as IC_{50} (nM), were obtained from the literature.[30−35] Chemical structures of selected CXCR2 antagonists were separated into training and test sets (Supplementary Tables 1 and 2, respectively) on the basis of activity and structural diversity. Three different chemical classes of CXCR2 inhibitors (*N,N′*-diarylsquaramides, *N,N′*-diarylureas, and *N,N′*-diarylguanidines; see Figure 1A) were chosen for pharmacophore hypothesis generation. The training and test sets have structurally similar sets of compounds and representatives from the three different classes to ensure structural diversity. The compounds are classified as highly active (IC_{50} < 0.01 μM, +++), moderately active (IC_{50} = 0.01−1 μM, ++), or inactive (IC_{50} > 1 μM, +) against CXCR2. Both the training and test sets have uniform distributions of compounds with these three activity classes. Our training set consisted of 20 compounds with significant structural diversity and a wide range of bioactivities, with IC_{50} ranging from 4 nM to 25 μM. Structures of compounds of a specified configuration were drawn using ChemDraw (version 12, PerkinElmer, Waltham, MA), and energy minimization was performed using open force field (OFF) methods with the steepest-descent algorithm within Discovery Studio 2.0 (Accelrys).[36] A gradient convergence value of 0.001 kcal/mol was used. Unique low-energy geometries generated were exported and minimized further using a modified CHARMM force field in Catalyst version 4.11[25] running on a Dell Precision T7400n Mini-Tower

computer with a dual quad-core Xeon X5450 processor and the Red Hat Linux 5.0 operating system. A maximum of 250 conformations for each compound were generated using the CHARMM force field parameters and the Poling algorithm[37] with the "best conformation generation" option and an energy threshold of 20 kcal/mol above the lowest-energy conformer to ensure maximum coverage of the conformational space.[38,39] All of the other parameters were set to default values. For generation of hypotheses using the HypoGen module in Catalyst, the minimum and maximum counts for the hydrogen-bond acceptor (HBA), hydrogen-bond donor (HBD), hydrophobic (HY), and aromatic ring (AR) features were set to 0 and 5 per feature type, respectively. The default uncertainty value of 3 was used for the compound activity, representing the ratio of the uncertainty range of the measured biological activity against the actual activity for each compound. An initial analysis of the function mapping tools revealed that the HBA, HBD, HY, and AR features effectively mapped all of the critical features of the training set compounds. Hence, the four features were selected to form the basis for the hypothesis generation process.

Pharmacophore Model Validation. Hypothesis models were used to predict the activities of the test set of known CXCR2 inhibitors (Supplementary Table 2). The geometric fit value for each of the test set compounds was calculated in order to predict the activity, which is a linear function of the fit value. The fit value is a quantitative term used to measure the number of features (HBA, HBD, HY, AR) mapped onto a compound and the distance that separates the feature on the molecule from the centroid of the hypothesis.[40] Fit values indicate how well features of a pharmacophore map the selected functional groups of a compound. The Güner−Henry (GH) scoring method[40] was used to calculate the "goodness of hit". To assess the quality of the pharmacophore models, a database of active and inactive inhibitors from the literature were evaluated with the equation below:

$$\text{GH score} = \frac{H_a(3A + H_t)}{4H_t A} \times \left[1 - \frac{H_t - H_a}{D - A} \right]$$

where D is the total number of compounds in the database, A is the number of actives, H_a is the total number of actives in the hit list, and H_t is the total number of compounds in the hit list. For this assessment, a database of known active and inactive inhibitors (previously published) was used to assess the pharmacophore.[30−32,34,35,41−55] GH scores were calculated for the top 10 hypotheses. The GH score values range from 0 (null model) to 1 (ideal model). A GH score greater than 0.7 indicates a good predictive model.[40]

Database Search. The best pharmacophore hypothesis (Hypo 1) was used as a search query to retrieve compounds with novel structural scaffolds and desired chemical features from a multiconformer Catalyst-formatted database consisting of 5 million commercially available compounds from Asinex (Moscow, Russia), Vitas-M Laboratory (Apeldoorn, The Netherlands), and Enamine (Kiev, Ukraine). The fast flexible search method in Catalyst was used to search the database.

Molecular Docking. Molecular docking studies were performed using GOLD version 5.2 in the allosteric site of the CXCR2 homology model obtained from GPCRR DB.[56] The C-terminal loop consisting amino acids 315 to 324 was refined using ModLoop.[57] This allowed automated refinement of the protein loop to make the allosteric site accessible to the solvent and ligand. The quality of the refined model was verified using
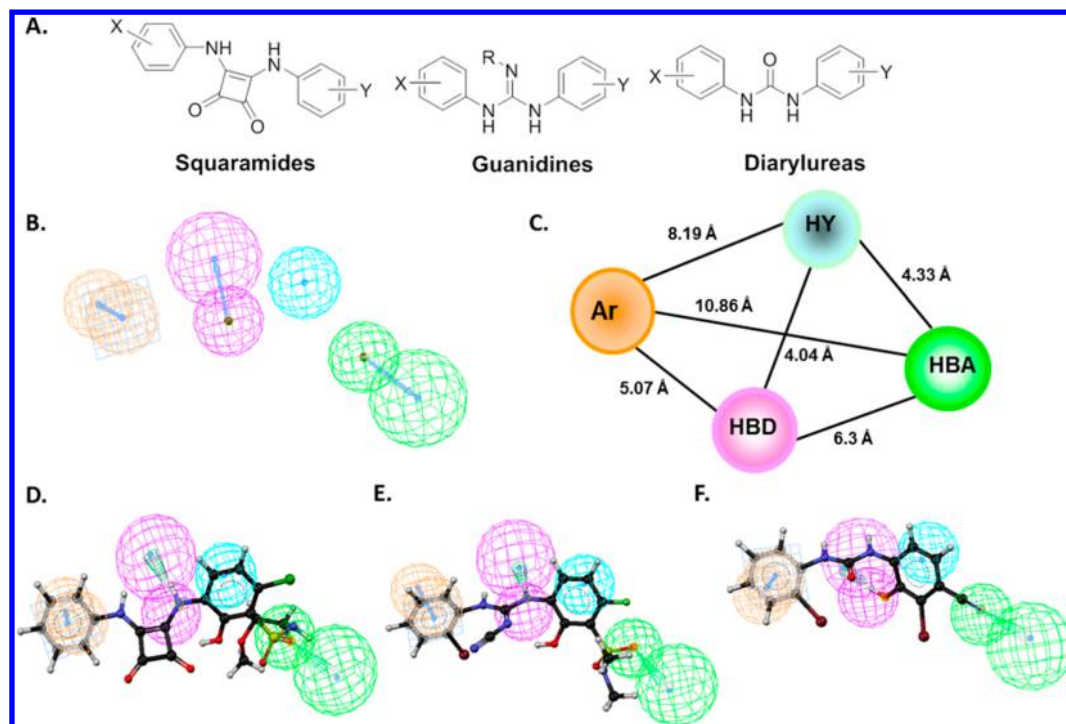
Figure 1. Pharmacophore modeling of Hypo-1. (A) The structural classes of CXCR2 inhibitors chosen for pharmacophore generation were squaramides, guanidines, and diarylureas. (B) The best hypothesis model, Hypo-1, was generated using the the HypoGen module in Catalyst (Accelrys). Pharmacophore features are shown in magenta for hydrogen-bond donor (HBD), cyan for hydrophobic group (HY), orange for aromatic group (AR), and green for hydrogen-bond acceptor (HBA). (C) Distances between pharmacophore features are given in angstroms. (D−F) Representatives of potent training set compounds chosen from three different classes of CXCR2 inhibitors are mapped onto Hypo-1: (D) squaramide **1**; (E) guanidine **7**; (F) diarylurea **13**.

Ramachandran plot within PROCHECK (http://services.mbi.ucla.edu/SAVES/). A total of 93.5% of the residues were predicted to be in the most favored region, and 6.5% of the residues were in the allowed regions, while none of the residues were in disallowed regions. Prior to docking, 10 different conformations were generated for each ligand using Omega (OpenEye Scientific Software), a systematic, knowledge-based conformer generator.[58] GOLD uses a genetic algorithm (GA) to explore the conformational space of a compound inside the binding site of a protein.[26,27] Docking studies were performed using the standard default settings with 100 GA runs on each molecule and allowing side-chain flexibility of important allosteric-site residues within their rotamer libraries.

Generation of the Shape-Based Pharmacophore. The shape-based pharmacophore was generated using ROCS version 3.2.0.4.[28,29] ROCS performs shape-based overlays of conformers from a candidate database on a query molecule with one or more conformations. Here we used a combination of shape overlap and color overlap by aligning groups with similar properties in the color force field. The score, called the Tanimoto Combo score, was calculated as the sum of the shape and color scores.[29] The maximum value of the Tanimoto Combo score is 2, and the minimum value is 0.

Cell Culture. The colon cancer cell lines HCT116 p53$^{+/+}$ and HCT116 p53$^{-/-}$ were kindly provided by Dr. Bert Vogelstein (Johns Hopkins Medical Institutions, Baltimore, MD). The NSCLC cell lines NCI-H1299, NCI-H460, and A549 were purchased from the National Cancer Institute (NCI) (Bethesda, MD). HCT116p53$^{+/+}$, HCT116 p53$^{-/-}$, H1299, H460, and A549 were grown in RPMI-1640 medium (Invitrogen, Carlsbad, CA) supplemented with 10% fetal bovine serum (FBS) at 37 °C

in a humidified atmosphere of 5% CO_2. CXCR2-bla and CXCR4-bla U2OS Tango cells were purchased from Invitrogen (Carlsbad, CA) and grown in McCoy's 5A medium supplemented with 10% dialyzed FBS, zeocin (200 μg/mL), hygromycin (50 μg/mL), Geneticin (100 μg/mL), sodium pyruvate (1 mM), nonessential amino acids (NEAA) (0.1 mM), and HEPES (25 mM). 293T cells overexpressing green fluorescent protein (GFP)-tagged CXCR2 (293T-CXCR2-GFP) were stably generated by Dr. Daryl Davies (University of Southern California School of Pharmacy, Los Angeles, CA) using a lentiviral system. 293T-CXCR2-GFP cells were cultured in Dulbecco's modified Eagle's medium (DMEM) (Invitrogen, Carlsbad, CA) supplemented with 10% FBS and puromycin (2 μg/mL). All of the cells were grown at 37 °C in a humidified atmosphere of 5% CO_2. All of the cell lines used were maintained in culture under 35 passages and tested regularly for *Mycoplasma* contamination using Plasmo Test (InvivoGen, San Diego, CA).

Compounds and Reagents. Compounds were purchased from Asinex and Enamine. Compounds were prepared as 10 mM stock solutions in dimethyl sulfoxide (DMSO) and stored at −20 °C. SB225002 and SB265610 were purchased from Tocris Bioscience (Ellisville, MI). Human CXCL8 cDNA was inserted into the expression vector pET32a at the EcoR1 and XhoI restriction site to generate His-tagged CXCL8. The sequence of the clone was confirmed by DNA sequencing. The recombinant CXCL8 was expressed in BL21-Gold (DE3) pLysS strain of *Escherichia coli* (Stratagene, La Jolla, CA) and purified using a previously reported protocol.[59]

CXCR2 and CXCR4 Tango Assay. CXCR2-bla U2OS cells stably overexpress CXCR2 linked to a tobacco etch virus (TEV) protease site and a GAL4-VP16 transcription factor. These cells

also stably express a β-arrestin-2/TEV protease fusion protein and a β-lactamase reporter gene. Upon CXCR2 activation in the presence of CXCL8, the β-arrestin-2/TEV protease fusion protein is recruited to the receptor and cleaves the peptide linker that links CXCR2 to the GAL4-VP16 transcription factor. Once cleaved, GAL4-VP16 may enter the nucleus and promote the transcription of the β-lactamase gene. β-Lactamase activity was detected using a fluorescence resonance energy transfer (FRET)-based fluorescence assay with CCF4-AM (Invitrogen). CCF4-AM is a β-lactamase FRET substrate and is cleaved in the presence of β-lactamase. The uncleaved substrate is excited at 409 nm and emits at 535 nm, whereas the cleaved substrate is excited at 409 nm and emits at 460 nm. Thus, the CXCR2 activity is directly correlated with the amount of cleaved β-lactamase substrate. In each assay, CXCR2 or CXCR4-bla U2OS cells were seeded (11000 cells/well) in 384-well tissue culture plates for 24 h in DMEM supplemented with 1% dialyzed FBS. Cells were pretreated with various concentrations of inhibitors for 30 min prior to the addition of CXCL8 (20 nM) or stromal-cell-derived factor 1 (SDF-1) (30 nM) and incubated for 5 h at 37 °C, unless otherwise noted in the figure legends. The β-lactamase substrate was loaded according to the manufacturer's protocol for 2 h, and plates were read on an Envision microplate reader (PerkinElmer) with excitation at 409 nm and emission at 460 or 540 nm. The ratio of cleaved (409/460) to uncleaved (409/540) was calculated for each sample well. The percent inhibition was calculated using the following formula:

$$\% \text{ inhib.} = \left[1 - \frac{\text{compound-treated} - \text{control}}{\text{CXCL8/SDF-stimulated} - \text{control}} \right] \times 100\%$$

where "control" refers to the unstimulated control.

Cell Proliferation. Cell proliferation was assessed by MTT assay as previously described.[60] In brief, cells were seeded in 96-well microtiter plates (3000−5000 cells/well) and allowed to attach overnight. The cells were continuously treated with compounds for 72 h. At the end of treatment, the cells were incubated with MTT solution (at a final concentration of 0.5 mg/mL) for 3 h at 37 °C. The supernatant was removed, and the cells were dissolved with 150 μL of DMSO. The absorbance was read at 570 nm on a microplate reader (Molecular Devices, Sunnyvale, CA). All of the experiments were performed in triplicate. IC$_{50}$ was determined for each compound from a plot of log(drug concentration) versus percentage of cells killed. The data reported with standard deviations are representative of at least three independent experiments.

CXCR2 In-Cell Western Assay. CXCR2-bla U2OS cells were seeded at 11000 cells/well in 384-well tissue culture plates in 40 μL of assay medium (DMEM supplemented with 1% dialyzed FBS) and incubated at 37 °C. The next morning, the assay medium was removed, and the cells were pretreated with 1× concentrations of CX compounds (36 μL total volume) for 30 min. Then 4 μL of 10× (10-fold concentrated) CXCL8 was added to each well (final concentration 50 nM), and the cells were incubated with CXCL8 for 1−5 h at 37 °C. The compounds and CXCL8 were removed, and the cells were fixed with 4% formaldehyde (25 μL/well) for 20−30 min at room temperature. The formaldehyde was removed, and the wells were washed with 1× phosphate-buffered saline (PBS) and stored at 4 °C. The next day, each well was blocked in blocking buffer (LI-COR, Lincoln, NE) for 2 h at room temperature and incubated with CXCR2 antibodies (Santa Cruz Biotechnology, 1:1000 dilution in blocking buffer) for 2 h at room temperature or overnight at 4 °C. The cells were then washed with 1× PBS six times and incubated with

mouse IRDye 680RD secondary antibodies (25 μL/well, 1:1000 dilution in blocking buffer) for 1 h in the dark. The wells were washed with 1× PBS six times to remove unbound antibodies. To remove excess liquid, the plates were spun upside-down on top of paper towels at 1200 rpm for 5 min. The plates were completely dried before imaging and quantification on the LI-COR Odyssey bioimager. To detect total CXCR2 expression (receptor degradation), cells were blocked in blocking buffer with 0.3% Triton X100 for 2 h. Primary and secondary antibodies were also diluted in 0.3% Triton X100 in blocking buffer. Percent inhibition of receptor internalization and degradation was calculated using the following formula:

$$\% \text{ inhib.} = \left[\frac{\text{compound-treated} - \text{CXCL8-stimulated}}{\text{control} - \text{CXCL8-stimulated}} \right] \times 100\%$$

where "control" refers to the unstimulated control.

Neutrophil Chemotaxis. Blood was collected from healthy human volunteers into EDTA-sprayed tubes (Greiner Bio-One, Monroe, NC). Human neutrophils were isolated using One-Step Polymorph separation medium (Accurate Chemical and Scientific, Westbury, NY) with centrifugation at 500 g for 35 min according to the manufacturer's recommendations. RBC lysis buffer (IBI Scientific, Peosta, IA) was used to remove residual erythrocytes. The final pellet of neutrophils was resuspended in Hank's balanced salt solution (HBSS) without Ca^{2+} or Mg^{2+} (Lonza, Walkersville, MD) supplemented with 1% bovine serum albumin (BSA) (Amresco, Solon, OH) and kept on ice. Neutrophils were quantified using Turk's blood diluting fluid (Ricca Chemical, Arlington, TX) and a hemocytometer. Trypan blue exclusion was used to determine neutrophil viability. All of the preparations consisted of approximately 95% viable neutrophils. All of the experiments were conducted with the approval of the University of Southern California Institutional Review Board.

Isolated neutrophils were incubated in triplicate with CX4152 over four logs of concentration or vehicle (1% DMSO) for 1 h. Neutrophils were then placed in the top wells of a 96-well MultiScreen-MIC plate with a pore size of 3 μm (Millipore, Billerica, MA) containing 50 nM CXCL8 in the bottom wells. Neutrophils were allowed to migrate for 2−4 h at 37 °C and 5% CO$_2$. In some experiments, the migrated neutrophils in the bottom wells were stained with Turk's blood diluting fluid and manually counted with a hemocytometer. In other experiments, the migrated neutrophils were labeled with CyQuant NF dye (Invitrogen, Eugene, OR), and the fluorescence intensity was measured using a spectrofluorometer (PerkinElmer) with excitation at 485 nm and emission at 530 nm. The neutrophil count was calculated using a standard curve. The percent of maximal chemotaxis (%MC) was calculated using the following formula:

$$\%MC = \left[\frac{N^{\text{treated}}_{\text{mig\_with\_CXCL8}} - N^{\text{untreated}}_{\text{mig\_without\_CXCL8}}}{N^{\text{untreated}}_{\text{mig\_with\_CXCL8}} - N^{\text{untreated}}_{\text{mig\_without\_CXCL8}}} \right] \times 100\%$$

in which $N^{\text{treated/untreated}}_{\text{mig\_with/without\_CXCL8}}$ is the number of treated/untreated cells migrated with/without CXCL8. The data were plotted using a sigmoidal E_{max} model to estimate the concentration associated with 50% inhibition of the maximal chemotactic response (IC$_{50}$).

Calcium Flux. 293T-CXCR2-GFP cells were seeded at 30000 cells/well in 384-well black plates with clear bottom plates in growth medium. The next day, the cells were loaded with Fluo-4 NW and probenecid according to the manufacturer's protocol (Invitrogen). Briefly, the dye mixture included in the kit

Table 1. Properties from Pharmacophore Hypothesis Generation Using Compounds from the Training Set

hypothesis[a]	total cost	error cost	RMS	correlation (R)	test set correlation (R)	features[b]
Hypo-1	89.43	74.13	0.83	0.93	0.79	HA, HD, HY, AR
Hypo-2	95.20	80.37	1.14	0.86	0.70	HA, HD, HY, AR
Hypo-3	95.83	80.84	1.16	0.86	0.69	HA, HD, HY, AR
Hypo-4	96.04	81.19	1.18	0.86	0.65	HA, HD, HY, AR
Hypo-5	96.81	81.62	1.20	0.85	0.76	HA, HD, HY, AR
Hypo-6	97.12	82.05	1.22	0.85	0.68	HA, HD, HY, AR
Hypo-7	97.25	82.40	1.23	0.84	0.64	HA, HD, HY, AR
Hypo-8	98.29	83.58	1.28	0.83	0.71	HA, HD, HY, AR
Hypo-9	98.44	83.25	1.26	0.83	0.72	HA, HD, HY, AR
Hypo-10	98.58	83.51	1.27	0.83	0.72	HA, HD, HY, AR

[a]Null cost = 121.34, fixed cost = 81.99, configuration cost = 13.59. All costs are in units of bits. [b]All of the pharmacophores consist of four features, including one each of hydrogen-bond acceptor (HA), hydrogen-bond donor (HD), hydrophobic (HY), and aromatic ring (AR).

was diluted with 10 mL of assay buffer and 100 μL of probenecid (25 mM final concentration). The growth medium was replaced with 25 μL of the dye mixture, and the cells were incubated at 37 °C for 30 min and at room temperature for 30 min (protected from light). To detect the calcium flux induced by the CX compounds, SB265610, or SB225002, 5× compound was added to each well, and the fluorescence signal was detected immediately on the Envision plate reader with 490 nm excitation and 535 nm emission filters. To detect CXCL8-stimulated calcium flux, 5× CX compounds and 5× CXCL8 (5 μL) were added to each well, and the fluorescence signal was detected immediately on the Envision plate reader with 490 nm excitation and 535 nm emission filters. The fluorescence signal was normalized to the baseline signal prior to any stimulation.

LPS-Induced Lung Inflammation. Eight- to ten-week-old male BALB/c mice were obtained from Charles River Laboratories and maintained in the animal facilities located at Zilkha Neurogenetic Institute (University of Southern California, Los Angeles, CA). A total of 12 mice with three in each treatment group (LPS alone or with CX4152 at 50, 5, or 0.5 mg/kg) were used for pharmacodynamic evaluation of lipopolysaccharide (LPS)-induced airway inflammation. Animals had access to food and water and were kept under controlled laboratory conditions with an average temperature of 22 °C and a light−dark cycle of 12 h. A single 0.25 mL injection containing CX4152 diluted in 5% DMSO in sesame oil or vehicle only (5% DMSO in sesame oil) was administered subcutaneously 30 min prior to LPS insufflation. All of the compounds were aseptically prepared. Acute lung in-flammation was induced by intranasal LPS insufflation (1 μg/20 g of body weight) under light sedation (100 μL of a ketamine (80 mg/kg) and xylazine (10 mg/kg) solution). Airway leukocytes were collected by bronchoalveolar lavage at 24 h. Bronchoalveolar lavage was performed after lethal intraperitoneal administration of Euthasol (75 mg/kg). The trachea was exposed through a midline incision with subsequent insertion of a 26G tracheal tube. The lungs were washed three times with three different aliquots of PBS (1 mL, 0.8 mL, 0.8 mL) with recovery via syringe aspiration of 86%. Bronchoalveolar lavage fluid (BALF) samples were placed on ice and centrifuged at 360g and 4 °C for 10 min. The cell pellet was used to evaluate the number of infiltrating leukocytes. Total and differential airway cell counts were determined for each BALF sample using a hemocytometer and Wright stain to examine nuclear morphology under the microscope. All of the animal work was conducted with the approval of the University of Southern California Institutional Animal Care and Use Committee (protocol no. 11675). All of the studies involving animals are reported in accordance with the ARRIVE guidelines.[61,62]

■ RESULTS

Development of a Robust CXCR2-Inhibitor-Based Pharmacophore Model. We chose three classes of previously described CXCR2 inhibitors (squaramides, guanidines, and diarylureas; Figure 1A) to develop pharmacophore models in order to identify novel compounds sharing similar chemical properties arranged in the same spatial orientation from a database of 5 million compounds. A pharmacophore is defined as a set of structural features in a drug molecule that is recognized at a receptor site and is responsible for its biological activity.[63] The most common pharmacophore features of a drug are hydrogen-bond donors and acceptors, hydrophobic regions, and
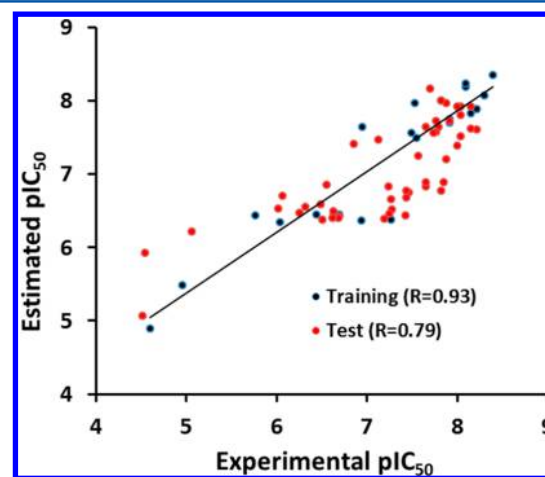

Figure 2. Graph showing the correlation between the experimental and predicted activities of 20 training set (black) and 50 test set (red) compounds.

Table 2. Hypo-1 Validation Using a Database of Previously Published CXCR2 Inhibitors

parameter	value
total no. of compounds in the database (D)	252
total no. of actives in the database (A)	153
total no. of hits (H_t)	132
no. of active hits (H_a)	122
% yield of actives	92.4
% ratio of actives in the hit list	79.7
enrichment factor (E)	1.5
no. of false negatives	31
no. of false positives	10
GH score (goodness of hit)	0.8

Table 3. CXCR2 Inhibition and Cancer Cell Proliferation Results of Active CX Compounds Selected from Hypo-1 Screening[a]

Compound Code	Structure	Fit	CXCR2 Inhibition (IC$_{50}$, μM)	CXCR4 Inhibition (IC$_{50}$, μM)	MTT (IC$_{50}$, μM)			
					H1299	H460	HCT116 p53$^{+/+}$	HCT116 p53$^{-/-}$
SB225002		6.69	0.19±0.24	>20	3.6±4.9	4.1±2.4	4.6±3.9	5.4±4.1
SB265610		6.72	0.28±0.09	>20	>50	>50	>50	>50
SB656933		7.4	NT	NT	NT	NT	NT	NT
SCH527123		6.5	NT	NT	NT	NT	NT	NT
CX25		6.4	0.36±0.1	0.59±0.1	8.0±6.5	3.9±1.5	3.9±1.9	6.2±5.2
CX86		5.81	1.1±1.4	3.4±3.3	7.3±4.8	6.1±2.3	3.8±0.5	5.5±2.2
CX815		6.15	0.4±0.1	>50	3.5±0.9	4.1±0.2	5.0±3.7	NT

[a]CXCR2 Inhibition was determined using the CXCR2 Tango assay. Cell proliferation was determined using the MTT assay. NT = not tested. Fit = fit value for Hypo-1. Each IC$_{50}$ value is the mean ± SD of two independent experiments in the CXCR2/4 Tango assay.
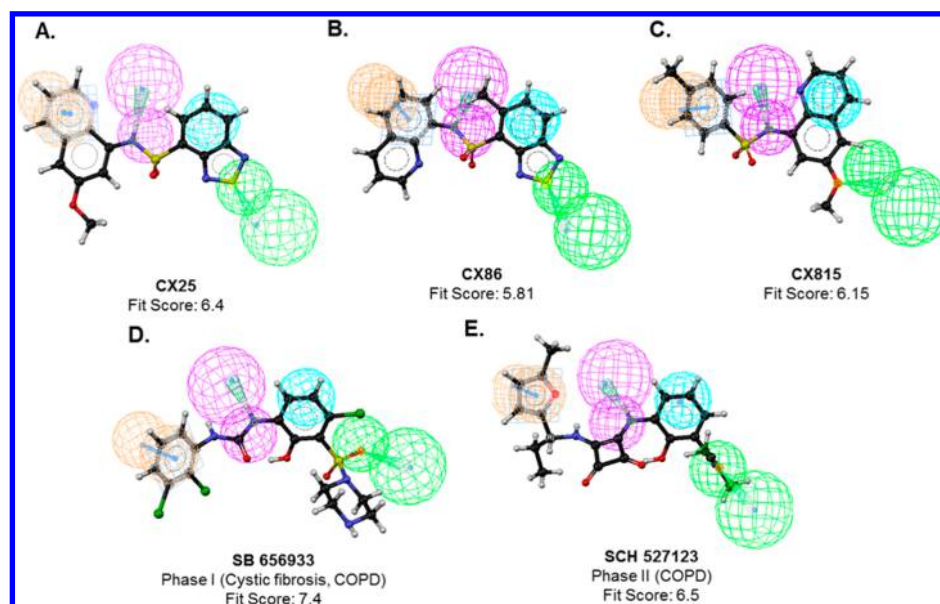
Figure 3. Pharmacophore mapping of CX compounds (A) CX25, (B) CX86, and (C) CX815 and CXCR2 inhibitors (D) SB656933 and (E) SCH527123 onto the Hypo-1 model with the indicated fit values.

cations/anions. Using a training set of 20 known CXCR2 inhibitors (Supplementary Table 1), we generated 10 quantitative pharmacophore models (Table 1) with the Catalyst software. All of the pharmacophore hypotheses consist of four chemical features: hydrogen-bond acceptor (HBA), hydrogen-bond donor (HBD), hydrophobic (HY), and aromatic ring (AR). We grouped the hypotheses into different clusters (Supplementary Table 3)

using the hierarchical complete linkage method. From the cluster analysis it is clear that although all of the pharmacophores contain four similar features, their arrangements are quite different. For instances, Hypo-1 and Hypo-2 are both in the same cluster up to a number of clusters equal to 6, but the HBD feature of Hypo-2 is different from that of Hypo-1 in the arrangement. In fact, all of the pharmacophores are different in terms of feature arrangement.
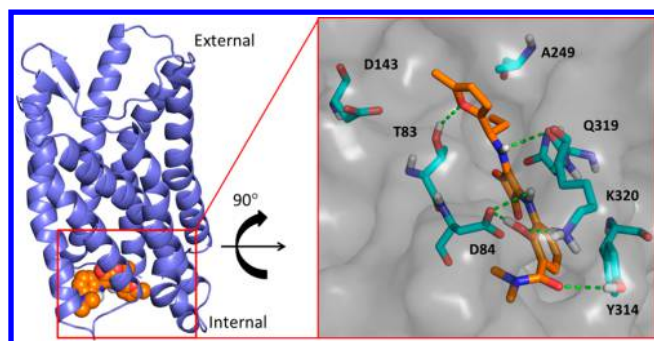
Figure 4. Docking of SCH527123 onto the allosteric site of CXCR2. (left) The seven transmembrane domains of the CXR2 homology model (blue) shown with SCH527123 (brown) docked onto the allosteric site located inside the receptor. (right) Zoomed docking pose of the inhibitor showing interactions with important allosteric site residues (cyan) within the receptor surface cavity (gray) after a 90° rotation in the horizontal plane. Green dotted lines indicate hydrogen-bonding interactions.

The best pharmacophore hypothesis, Hypo-1 (Figure 1B,C), was selected for further investigation on the basis of its statistical parameters (Table 1).

The value of the total cost of each hypothesis was much closer to the fixed cost value, which is expected for a good hypothesis. The difference between the null hypothesis cost and the fixed cost and the difference between the null hypothesis cost and the total cost of the best hypothesis (Hypo-1) were 39.35 and 31.91 bits, respectively. The entropy (configuration cost) value of 13.59 for the hypothesis is also within the allowed range of 17.00.[64] Experimental and estimated activity data for both the training and test set compounds are plotted as shown in Figure 2 and are reported in Supplementary Tables 1 and 2, respectively. Hypo-1 has excellent predictive ability for the test set compounds (correlation coefficient $R = 0.79$). Most of the test compounds are predicted with error values of less than 5. For further validation of our pharmacophore model, a database of 252 molecules consisting of 153 actives ($IC_{50} \leq 100$ nM) and 99 inactives ($IC_{50} \geq 1$ μM) that were previously reported in the literature were screened with Hypo-1.[30−32,34,35,41−43] We did not consider moderately active compounds (100 nM to 1 μM) in the validation database in order to clearly distinguish between actives and inactives. GH scores were calculated to show the robustness of all 10 pharmacophore models (Supplementary Table 4). Hypo-1 successfully retrieved 80% of the actives from the database (Table 2). A GH score of 0.80 indicates a model of significantly good quality.[40]

Hypo-1 was mapped onto the three highly active and structurally diverse classes of CXCR2 inhibitors (squaramides, guanidines, and diarylureas) with an excellent fit value (>8) (Figure 1D−F). Aromatic and hydrophobic features are mapped onto two phenyl groups of the active training set compounds, while hydrogen-bond donor and acceptor are mapped onto one of the amine groups and a sulfonyl oxygen or cyano group, respectively. Although an *o*-hydroxyl group in one of the phenyl rings is the most common in the training set, our best model did not identify that feature except in a few cases (the OH group in compound **13** is partially mapped onto the hydrogen-bond donor feature; Figure 1F). There are several other pharmacophores, such as Hypo-2, Hypo-3, and Hypo-4, that also mapped onto that hydroxyl group, but they were not the best pharmacophore in terms of pharmacophore parameters and external validation (Table 1 and Supplementary Table 4). Hypo-1 was

used to screen a database of 5 million commercially available compounds from Asinex, Enamine, and Vitas-M Laboratory.[65−67] The criteria for virtual screening were as follows: (a) the fit value should be >5 and (b) the compound should map all of the features of the pharmacophore. This yielded 350 compounds with fit values >5. These compounds were chosen for cell-based screening in the CXCR2 Tango assay.

Identification of CX Compounds in CXCR2 Screening. Using the CXCR2 Tango assay, we initially screened 144 compounds from 350 pharmacophore hits based on structural diversity as well as commercial availability. Thirteen compounds belonging to the class of sulfonamides were identified as hits from our initial screen. The best initial hits identified from pharmacophore screening are presented in Table 3 and mapped onto the Hypo-1 pharmacophore model in Figure 3. Our most active hit compound, CX25 ($IC_{50} = 360 \pm 100$ nM) was chosen for further lead optimization. These compounds were also counterscreened
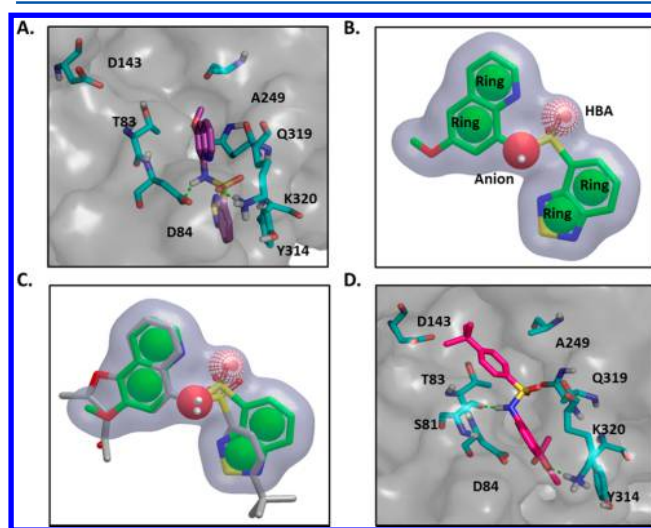

Figure 5. Lead optimization performed using docking and generation of the shape-based pharmacophore of CX25. (A) CX25 is docked onto the allosteric site of CXCR2 (gray-colored receptor surface). Asp84 and Lys320 form hydrogen-bonding interactions with CX25 (purple), while Tyr314 is involved in π−π interactions. Several other residues, such as Thr83, Ala249, and Gln319, form hydrophobic interactions with CX25. (B) A six-feature shape-based pharmacophore comprising four rings, one anion, and one hydrogen-bond acceptor (HBA) was generated with ROCS using the docking pose conformation of CX25. (C) The ROCS pharmacophore is mapped onto CX4152 with a ROCS Tanimoto Combo score of 1.028. (D) CX4152 (pink) is docked onto the allosteric site of CXCR2. It forms two hydrogen bonds with Ser81 and Lys320 and hydrophobic and π−π interactions with other important residues.
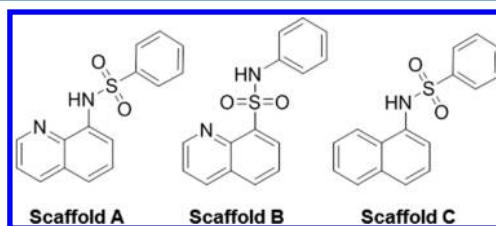

Figure 6. Chemical structures of scaffolds A−C. Compounds with scaffold A were the most active in the CXCR2 Tango assay. All of the compounds with scaffold B were inactive. Compounds with naphthalene instead of quinoline (scaffold C) were slightly less active than compounds with scaffold A, suggesting the importance of the nitrogen in the quinoline structure.

in the CXCR4 Tango assay. Interestingly, most of the active CX compounds also inhibited CXCR4 activity in the Tango assay. For example, CX25 inhibited CXCR4 with IC$_{50}$ = 0.59 ± 0.1 μM.

Lead Optimization and Structure−Activity Relationship Analysis. Given that some of the CXCR2 inhibitors used to derive Hypo-1 were later shown to act allosterically, we decided to dock CX25 onto the allosteric site of the CXCR2

homology model.[56,68] We validated our docking model using a clinical candidate, SCH527123. The predicted binding mode of the inhibitor exhibited interactions with the important residues Thr83, Asp84, Ala249, Tyr314, Gln319, and Lys320, in agreement with mutagenesis studies (Figure 4).[69] From our docking studies, CX25 was predicted to bind in the allosteric site, where it forms hydrogen-bonding interactions with Asp84 and Lys320

Table 4. CXCR2 Inhibition and Cancer Cell Proliferation Results for CX Compounds with Scaffold A Selected from the ROCS Pharmacophore of CX25[a]

Compound Code	Structure	Fit	ROCS score	CXCR2 Inhibition (IC$_{50}$, μM)	CXCR4 Inhibition (IC$_{50}$, μM)	MTT (IC$_{50}$, μM)		
						H1299	H460	HCT116p53+/+
CX692		5.99	1.407	5.0±6.3	0.6	3.6±2.0	3.3±1.1	NT
CX122		6.01	1.398	2.1±1.7	2.8±1.7	2.3±1.7	1.7±1.4	4.5
CX595		5.83	1.329	2.1±1.5	2.6±1.8	2.4±1.6	1.4±1.0	5.0
CX295		5.84	1.401	4.0±0	5.1±2.8	2.0±1.9	1.7±2.0	NT
CX857		6.04	1.396	4.5±4.9	4.7±10.9	NT	NT	NT
CX748		6.01	1.376	3.0±1.4	3.0±2.8	1.4±1.6	1.5±2.1	1.6
CX721		5.94	1.272	4.5±0.7	21.0±26.6	>20	>20	>20
CX279		6.03	1.396	2.2	3.0±1.4	2.1±1.8	2.2±1.8	1.6
CX684		5.94	1.387	1.4±1.1	1.0±0.6	1.2±0.7	0.9±0.7	2.5
CX061		6.18	1.33	2.5±1.7	2.5±1.9	2.3±1.9	1.5±1.1	3.3
CX297		5.88	1.388	2.4±2.3	3.6±1.2	3.0±0.7	4.1±1.3	NT
CX296		5.82	1.459	5.6±3.2	20.7±17.2	45.0±7.3	70.8	NT

Table 4. continued

Compound Code	Structure	Fit	ROCS score	CXCR2 Inhibition (IC$_{50}$, μM)	CXCR4 Inhibition (IC$_{50}$, μM)	MTT (IC$_{50}$, μM)		
						H1299	H460	HCT116p53+/+
CX388		6.13	1.149	1.6	5.0	3.2	5.0	14
CX310		5.86	1.279	1.6±1.2	NT	NT	NT	8.2
CX324		5.86	1.075	3.1±2.7	4.8±3.2	3.0±1.4	2.6±1.4	NT
CX128		5.9	0.882	2.4±2.3	<0.2	>10	>10	NT
CX826		6.16	1.349	1.7±2.0	7.1	1.4±1.0	0.9±0.6	5.0
CX073		6.06	1.255	7.0±6.1	>20	20.0	17.8	NT
CX587		6.21	1.296	5.0	NT	8.5±0	>10	NT

[a]CXCR2 inhibition was determined using the CXCR2 Tango assay. Cell proliferation was determined using the MTT assay. NT = not tested. Fit = fit value for Hypo-1. ROCS score = Tanimoto Combo score for the ROCS pharmacophore. Each IC$_{50}$ value is the mean ± SD of at least two independent experiments in the CXCR2/4 Tango assay.

(Figure 5A). The benzothiadiazole ring system of CX25 formed a π−π interaction with Tyr314, whereas the quinoline ring system formed hydrophobic interactions with Thr83, Ala249, and Gln319 (Figure 5A). The docked conformation and pharmacophore alignment of CX25 are quite similar. Three of the four Hypo-1 features were reproduced in the docking of CX25. We observed a hydrogen-bonding interaction between the sulfonyl oxygen and Lys320 in the docking model. The contribution of this interaction to the activities of compounds needs further investigation. Although the sulfur atom in the thiadiazole ring was recognized by Hypo-1 as a hydrogen-bond acceptor, docking of CX25 did not reveal any interaction with the S atom. A shape-based pharmacophore (Figure 5B) was generated on the basis of the docking pose of CX25 and its interactions with the binding site residues using ROCS.[28,29] The pharmacophore consists of four rings, one anion, and one hydrogen-bonding interaction, which mimics the docking interactions of CX25. On the basis of the docking and HypoGen pharmacophore models, we concluded that the sulfonamide NH acts as a hydrogen-bond donor, but ROCS does not consider this as a hydrogen-bond donor. Instead, ROCS considers this an anion. The ROCS pharmacophore retrieves not only compounds with similar features but also compounds with three-dimensional similarity. We further
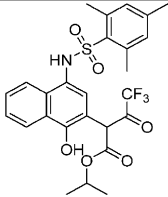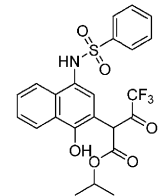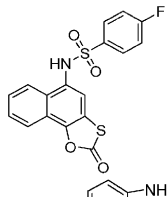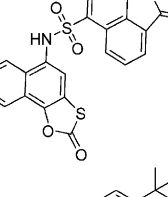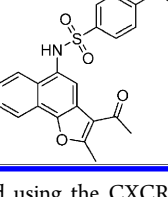
identified and tested 103 additional sulfonamides from the shape-based pharmacophore search containing an NH group, a feature recognized by the ROCS pharmacophore as an anion. Our docking model accurately recognizes the NH functionality as a hydrogen-bond donor.

Testing of these compounds in the same assay as described above resulted in 33 compounds with IC$_{50}$ values of <10 μM. Most of the tested compounds are categorized by three scaffolds, denoted as scaffolds A−C (Figure 6). Several compounds with scaffolds A and C showed significant inhibitory activity in the CXCR2 assay (Tables 4 and 5). However, none of the compounds with scaffold B showed significant activity (Supplementary Table 5). The inactive compounds containing scaffolds A and C are listed in Supplementary Table 6. Overall, compounds having scaffold A were most active, exhibiting IC$_{50}$ values in the nanomolar to low-micromolar range. Halogen substitution (Cl, Br, F, or CF$_3$) on the benzene ring in scaffold A enhanced the activity. The polar thiadiazole ring structure on the benzene (CX25 and CX86) also improved the activity by providing a hydrogen-bond acceptor group (S) between the ortho and meta positions. This observation supports our current pharmacophore model, which predicts that a hydrogen-bond acceptor group on the hydrophobic benzene group is essential for activity. However,

Table 5. CXCR2 Inhibition and Cancer Cell Proliferation Results for CX Compounds with Scaffold C Selected from the ROCS Pharmacophore of CX25[a]

Compound Code	Structure	Fit	ROCS score	CXCR2 Inhibition (IC$_{50}$, μM)	CXCR4 Inhibition (IC$_{50}$, μM)	MTT (IC$_{50}$, μM)	
						H1299	H460
CX309		6.37	1.105	16.5±1.1	8.9	6.2±5.6	>20
CX640		6.33	1.142	8.4±4.6	NT	>10	>10
CX078		7.18	1.085	8.0±6.8	10.0	NT	NT
CX459		6.46	0.743	3.6±6.9	11.7	8.3±8.2	17.8
CX910		7.05	0.960	>20	NT	NT	NT
CX588		7.74	0.757	3.6	NT	NT	NT
CX886		7.76	0.748	7.9	NT	3.6±0.6	15.8
CX887		6.57	0.974	15.4±1.1	8.9	NT	NT
CX410		6.54	0.923	17.8	NT	5.0±0	>10

Table 5. continued

Compound Code	Structure	Fit	ROCS score	CXCR2 Inhibition (IC$_{50}$, μM)	CXCR4 Inhibition (IC$_{50}$, μM)	MTT (IC$_{50}$, μM)	
						H1299	H460
CX396		6.34	0.849	6.5±8.7	7.6	NT	NT
CX404		6.34	0.668	11.1±6.8	20	NT	NT
CX474		6.42	1.194	16.3±3.4	>20	20.0	>20
CX489		7.12	1.178	>20	NT	NT	NT
CX4152		6.21	1.028	7.6±6.2	64.7±18.9	31.6	20.0

[a]CXCR2 inhibition was determined using the CXCR2 Tango assay. Cell proliferation was determined using the MTT assay. NT = not tested. Fit = fit value for Hypo-1. ROCS score = Tanimoto Combo score for the ROCS pharmacophore.

other substitutions with acetyl, acetylamine, sulfonamide, and methoxy groups at the para position on the benzene ring significantly decreased the activity. Mono-, bis-, and trismethylation of the benzene did not improve the activity. However, isopropyl substitution improved the activity 4-fold. We also observed that methoxy substitution on the quinoline significantly improved the activity of compounds with scaffold A. For example, the methoxy substitution on the quinoline in CX25 improved its activity (IC$_{50}$ = 360 nM) compared with CX86 (IC$_{50}$ = 1.1 μM).

All of the compounds with scaffold B were inactive at 10 μM (Supplementary Table 5). For example, compound CX624 was inactive at 10 μM, whereas compound CX061 (scaffold A) had an IC$_{50}$ value of 2.5 μM. These data suggest that the NH group (hydrogen-bond donor) on the quinoline is essential for activity, as it is a significant pharmacophoric feature. Compounds with naphthalene instead of quinoline (scaffold C; Table 5) were slightly less active than compounds with scaffold A, suggesting the importance of the nitrogen in the quinoline structure. Although there is no interaction between the quinoline nitrogen and the active-site residues in our docked model, the importance of the quinoline may be attributed to its physicochemical properties affecting cell permeability and solubility, leading to slightly better activities than for the naphthalene analogues.

CX4152 Is Selective for CXCR2 over CXCR4. CX4152 (Table 5 and Figure 7A) showed better selectivity for CXCR2 (IC$_{50}$ = 7.6 ± 6.2 μM) over CXCR4 (IC$_{50}$ = 64.7 ± 18.9 μM) in the Tango assays (Figure 7B) and was selected for further mechanistic studies. Figure 7C shows that the order of addition of CX4152 and CXCL8 affects the potency of CX4152 in the CXCR2 Tango assay. CX4152 showed greater potency when CXCR2-bla U2OS cells were pretreated with CX4152 for 30 min prior to CXCL8 stimulation than when the cells were cotreated with CX4152 and CXCL8 at the same time. CX4152 is mapped onto the ROCS pharmacophore with a Tanimoto Combo score of 1.028 (Figure 5C) and also fits well into the Hypo-1 pharmacophore model with a fit value of 6.21 (Figure 7D). When CX4152 is docked onto the allosteric site of CXCR2 it forms hydrogen-bonding interactions with Ser81 and Lys320, hydrophobic interactions with Thr83, Ala249, and Gln319, and π−π interactions with Tyr314 (Figure 5D). The docking pose of CX4152 reproduces four out of four Hypo-1 features as well as five out of six ROCS pharmacophore features. We also performed similarity searches with CX4152 and found additional compounds that exhibit similar chemical features and shapes. However, these analogues were not more potent than CX4152 and showed less CXCR2 selectivity (Table 6).
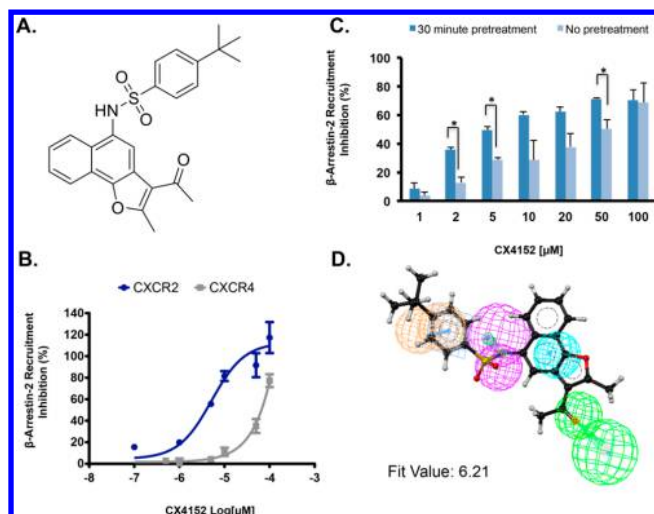
Figure 7. CX4152 selectively inhibits CXCR2. (A) Chemical structure of CX4152. (B) CX4152 is mapped onto Hypo-1 with a fit value of 6.21. (C) Dose−response curves of CX4152 in the CXCR2 and CXCR4 Tango assays. Cells were pretreated with various doses of CX4152 for 30 min prior to CXCL8 (30 nM) stimulation for 5 h. (D) CX4152 inhibits CXCR2 in the Tango assay in a time-dependent manner. Cotreatment with CX4152 and CXCL8 reduced the potency of CX4152 in the CXCR2 Tango assay compared with pretreatment of cells with CX4152 for 30 min prior to CXCL8 stimulation. Each data point represents the mean ± SD of a representative experiment performed in duplicate. * indicates $p < 0.05$.

CX4152 Induces CXCR2 Internalization. To characterize the mechanism of CX4152, we assessed its effects on receptor internalization using in-cell Western assays. CX4152 induced receptor internalization in a dose- and time-dependent manner (Figure 8A,B). We also observed a decrease in total CXCR2 after 5 h of treatment (Figure 8C,D). Increases in total CXCR2 receptor were observed at earlier time points. Treatment with CX25 and SB265610 did not induce receptor internalization as observed with CX4152 (Figure 9).

CX4152 Does Not Induce Calcium Mobilization. Since we showed that CX25 induced rapid calcium mobilization in lung and colon cancer cells, we also assessed the effects of CX4152 on calcium mobilization. CX4152 did not induce rapid calcium mobilization in CXCR2-overexpressing cells (293T-CXCR2-GFP), whereas CX25 induced peak calcium flux within 1 min of stimulation (Figure 10). SB265610 alone did not have any effect on calcium mobilization. Stimulation with 300 nM CXCL8 rapidly induced transient calcium mobilization. SB265610 inhibited CXCL8-induced calcium flux, as indicated by a reduced calcium peak when cells were costimulated with SB25610 and CXCL8. CX4152 had no effect on CXCL8-induced calcium flux.

CX4152 Inhibits Cell Proliferation. We further assessed the cellular effects of CX4152 on proliferation of CXCR2-expressing cells (293T-CXCR2-GFP and CXCR2-bla U2OS) and their parental cell lines (293T and U2OS, respectively) as well as CXCR4-expressing (CXCR4-bla U2OS) and NSCLC (A549, H460, and H1299) cell lines. CX4152 inhibited cell proliferation (72 h of treatment) in all of the cell lines tested with similar IC_{50} values for the CXCR2-overexpressing and parental cell lines, suggesting that the effects on cell proliferation may not be CXCR2-mediated (Table 7).

CX4152 Inhibits PMN Cell Migration. Finally, to assess the antichemotactic effects of CX4152, we measured human neutrophil chemotaxis toward 50 nM CXCL8 using a modified

Boyden chamber transwell assay. We previously determined that 50 nM CXCL8 is an optimal concentration (data not shown). CX4152 inhibited CXCL8-induced chemotaxis in a concentration-dependent manner with an IC_{50} value of 51 μM (Figure 11A). More importantly, 50 mg/kg CX4152 was able to significantly inhibit polymorphonuclear leukocyte (PMN) migration (about a 2-fold decrease) using a murine model of neutrophilic airway inflammation induced with LPS (Figure 11B).

■ DISCUSSION AND CONCLUSIONS

The identification of compounds that modulate CXCR2 function was facilitated by computational studies using a CXCR2-inhibitor-based pharmacophore model, Hypo-1. This model exhibits high predictive power to identify CXCR2 inhibitors with a test set correlation between the predicted and experimental activities of 0.79 (Table 1 and Figure 2) and a good GH score (0.80). This model discriminates between actives (fit value >5) and inactives in an in-house database of CXCR2 inhibitors, reducing the need to perform large-scale in vitro screening studies (Table 2). Virtual screening of a commercially available database of 5 million compounds with Hypo-1 retrieved 350 compounds with fit values of >5. Thirteen out of 144 compounds selected for in vitro screening showed IC_{50} values of <10 μM, a hit rate of 9.7%. Of these, CX25 was the most potent, inhibiting CXCR2 activation with an IC_{50} value of 360 nM, and was selected for further studies to characterize its effects in cancer cell lines (Table 3). Hypo-1 also identified four chemical features (hydrogen-bond donor, hydrophobic, hydrogen-bond acceptor, and aromatic ring) that are important for CXCR2 inhibition. The location of these chemical features is important for the activity, as clearly demonstrated with scaffolds A and B. The activity was abolished when the hydrophobic group (benzene) and the aromatic group (quinoline/naphthalene) on the sulfonamide backbone were swapped.

CX compounds showing nanomolar activity against CXCR2 in the Tango assay (CX25, CX86, CX815, and CX122) also inhibited cell migration, proliferation, and colony formation in cancer cell lines with similar potencies as SB225002 (Supplementary Figures 1−3). Additionally, we observed that SB225002 arrested cells in the G2/M phase, which is inconsistent with previous studies showing that CXCR2 knockdown in ovarian cancer cell lines arrested cells in the G0/G1 phase (Supplementary Figure 4).[18] However, SB265610, a derivative of SB225002 that is just as potent as SB225002 at inhibiting CXCR2 in the Tango assay, did not show cytotoxicity in any cell lines tested and inhibited cell proliferation less than 50% at 50 μM. This is consistent with previous studies showing that CXCR2 knockdown with shRNA in melanoma cells reduced cell proliferation by 40% in low serum.[70] CX compounds arrested the cell cycle in the S phase in NSCLC cell lines and in the G2/M phase in colon cancer cell lines (Supplementary Figure 4). This suggests that the toxicity observed with CX compounds and SB225002 may not be CXCR2-mediated but rather may be an off-target effect of these compounds. Indeed, SB225002 was recently shown to exhibit microtubule destabilizing activity by binding to tubulin and inducing mitotic arrest in p53 mutant cancer cell lines.[71,72] It was also reported that SB265610 did not induce G2/M cell cycle arrest at concentrations as high as 100 μM. This indicates that the slight difference in the chemical structures of SB225002 and SB265610 dramatically alters the off-target effects of inhibitors belonging to the diarylurea class.

This further suggests that the Hypo-1 pharmacophore model may also capture compounds exhibiting off-target effects that are

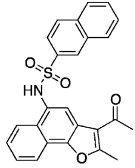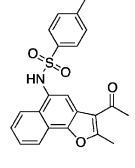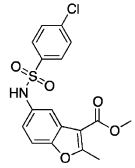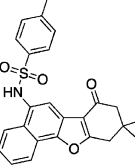**Table 6. Inhibition of CXCR2 and CXCR4 Activation and Cytotoxicity of CX4152 Analogues**
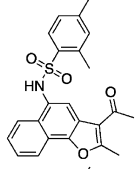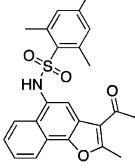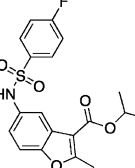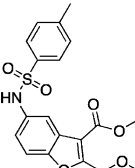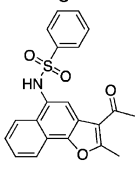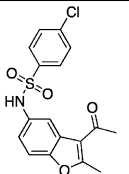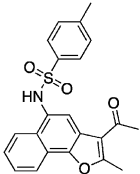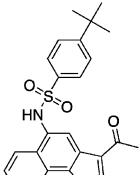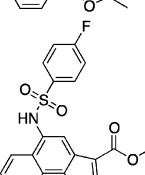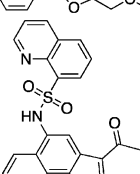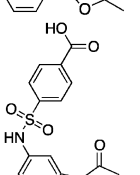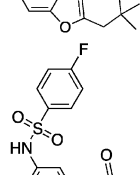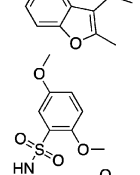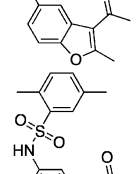
Compound Code	Compound	ROCS score	CXCR2 (IC$_{50}$, µM)[a]	CXCR4 (IC$_{50}$, µM)[a]	MTT (IC$_{50}$, µM)[b]				
					293T-CXCR2	293T	H460	H1299	A549
CX8794		1.029	40±13.2	4	2	2.5	3.1	3.5	3.5
CX8793		1.012	28.3±22.5	1	<1	<1	2	2.7	1.1
CX4083		1.005	44±26.5	12	23	19	26	12	38
CX8843		0.993	40±28.3	35	NT[c]	NT	NT	NT	NT
CX8788		1.118	10±0	10	30	30	25	23	40
CX8789		1.092	28.3±7.6	6	60	>100	>100	40	70
CX4138		0.955	27.5±24.7	18	36	33	22	29	39
CX0965		0.833	32±39.6	1	1.1	3	3.5	4	4
CX0572		1.12	52.3±44.5	30	NT	NT	NT	NT	NT

Table 6. continued

Compound Code	Compound	ROCS score	CXCR2 (IC$_{50}$, μM)[a]	CXCR4 (IC$_{50}$, μM)[a]	MTT (IC$_{50}$, μM)[b]				
					293T-CXCR2	293T	H460	H1299	A549
CX0570		1.05	12.4±11.5	25	4.6	4.5	4.7	5	7
CX0562		1.053	18.7±22.8	6	NT	NT	NT	NT	NT
CX8787		1.028	6.3±1.1	30	20	55	10	55	60
CX0994		1.022	>100	NT	NT	NT	NT	NT	NT
CX8226		1.05	>100	NT	NT	NT	NT	NT	NT
CX8732		0.867	>100	NT	NT	NT	NT	NT	NT
CX7769		1.025	>100	NT	NT	NT	NT	NT	NT
CX6232		0.781	>100	NT	NT	NT	NT	NT	NT
CX4093		1.047	>100	NT	NT	NT	NT	NT	NT

[a]Each IC$_{50}$ value is the mean ± SD of three independent experiments in the CXCR2/4 Tango assay. [b]Cells were treated with compounds for 72 h, and cell proliferation was measured using the MTT assay. [c]NT = not tested. ROCS score = Tanimoto Combo score for the ROCS pharmacophore.
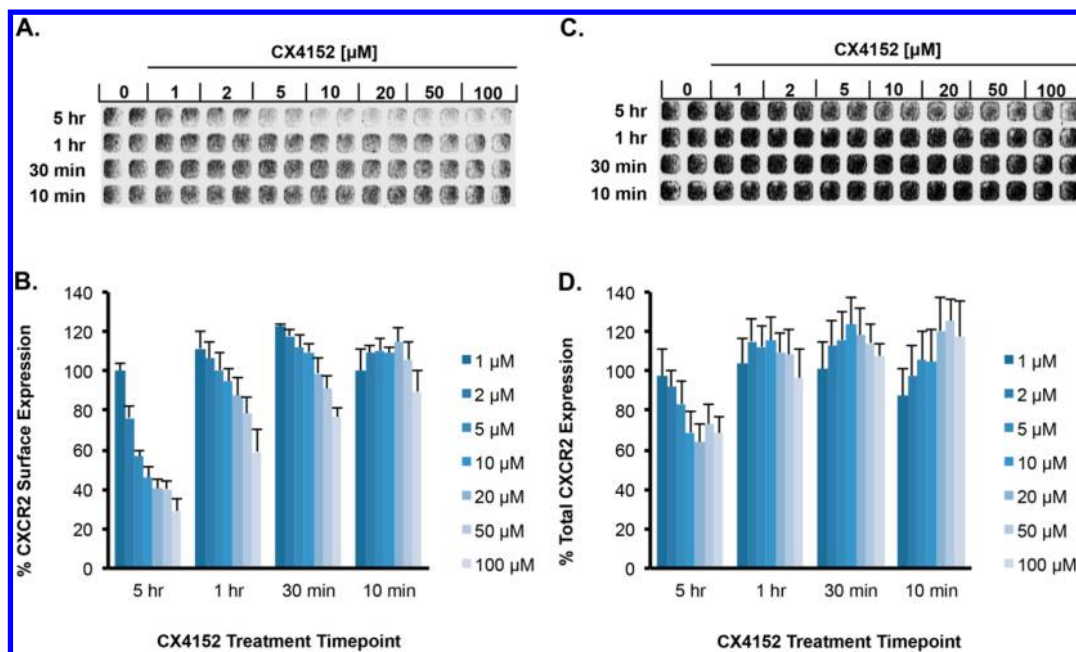
Figure 8. CX4152 induces CXCR2 internalization and turnover. CXCR2 surface and total expression was measured using a CXCR2 receptor in-cell Western assay. CXCR2-bla U2OS cells were treated with CX4152 at indicated concentrations for various times. (A) CX4152 dose- and time-dependently reduced CXCR2 surface expression. (B) Quantification of the data shown in (A). Each value represents the mean ± SD of a representative set of at least three independent experiments performed in duplicate. (C) CX4152 reduced the total CXCR2 expression at the 5 h time point. (D) Quantification of the data in (C). Each value represents the mean ± SD of a representative set of at least three independent experiments performed in duplicate.
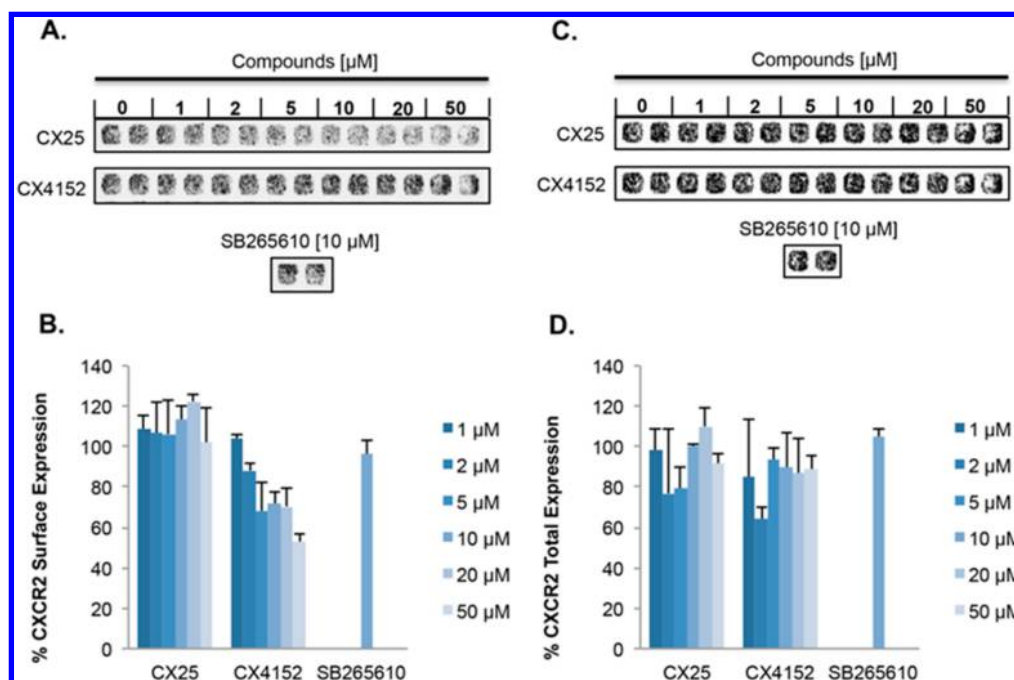

Figure 9. CX25 does not induce CXCR2 internalization and turnover. CXCR2-bla U2OS cells were treated with various doses of CX25 and CX4152 for 1 h. Cells were also treated with 10 μM SB265610 for 1 h. (A) Surface and (B) total expression of CXCR2 were assessed using the CXCR2 receptor in-cell Western assay. Quantification of the data in (A) and (B) shows that CX25 and SB265610 treatment did not reduce (C) surface and (D) total CXCR2 expression.

inherent in the CXCR2 inhibitors (training set) used to generate Hypo-1. We propose that the cytotoxicity of CX25 may be due to its effects on calcium release. CX25 induced a rapid burst of intracellular calcium release in a dose-dependent manner (5−20 μM) in lung and colon cancer cells (Supplementary Figure 5), whereas SB225002 and SB265610 only slightly induced calcium at higher

concentrations (20 μM). Calcium signaling is a key component of apoptotic signaling. Agents that increase intracellular free calcium, such as thapsigargin (SERCA inhibitor) and ionomycin (calcium ionophore), have been shown to induce apoptosis.[73,74]

A counterscreen with another chemokine receptor, CXCR4, showed that CX compounds also inhibited CXCR4 with similar
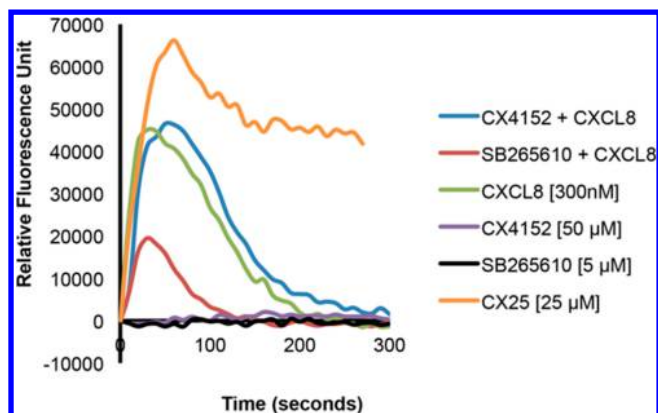
Figure 10. Calcium response curves of CX4152, CX25, and SB265610 in CXCR2-overexpressing cells. 293T-CXCR2-GFP cells were stimulated with CX4152 (50 μM), SB265610 (5 μM), CX25 (25 μM), or CXCL8 (300 nM). Cells were also costimulated with CX4152 (50 μM) and CXCL8 (300 nM) or SB265610 (5 μM) and CXCL8 (300 nM). CX4152 alone did not induce calcium mobilization and had no effect on CXCL8-mediated calcium mobilization.

Table 7. Cytotoxicity of CX4152 in a Panel of Cancer Cell Lines[a]

cell line	MTT IC$_{50}$ (μM)
293T	24.5 ± 6.4
293T-CXCR2	21 ± 9.9
CXCR2-bla U2OS	42, >50
CXCR4-bla U2OS	44, >50
U2OS	37.5 ± 9.2
A549	21 ± 9.9
H460	20
H1299	31.6

[a]Each IC$_{50}$ value is the mean ± SD of two or three independent MTT experiments performed in triplicate. Cells were treated with compounds for 72 h, and cell proliferation was measured using the MTT assay.

potencies, suggesting that these compounds are not very selective for CXCR2 and may target other chemokine receptors as well as similar classes of GPCRs. Additional structure–activity relationship studies and optimization of these compounds may improve their selectivity. Thus, we performed additional shape-based ROCS pharmacophore searches and screening. We identified CX4152 to be 8 times more selective for CXCR2 over CXCR4 in the Tango assay, with IC$_{50}$ values of 7.6 ± 6.2 and 64.7 ± 18.9 μM, respectively. CXCR2 and CXCR4 belong to the same chemokine family and are activated by different ligands. All of the components of the CXCR2 and CXCR4 Tango assays are identical except for chemokine receptor expression in the Tango cell lines and ligand activation. Thus, we do not anticipate selectivity in CXCR2/4 Tango assays if β-arrestin-2 is the target of inhibition or if the compounds target any component of the assay (i.e., fluorescence readout or reporter gene expression). As observed with SB265610 and SB225002, CX4152 exerts very different cellular effects than CX25 despite sharing similar chemical backbone structure, further demonstrating that slight chemical modifications can dramatically alter off-target effects and perhaps the selectivity. CX4152 reduced cell proliferation in a panel of cell lines with high and low CXCR2 expression (Table 7), suggesting that the antiproliferative effects of CX4152 are most likely CXCR2-independent, perhaps targeting other
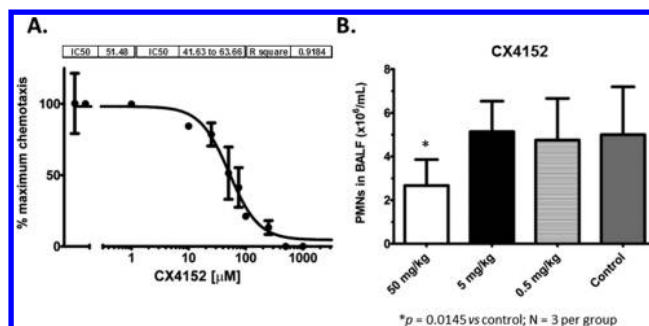

Figure 11. CX4152 inhibits CXCL8-mediated cell migration. (A) Concentration-dependent inhibition of human neutrophil chemotaxis. Neutrophils were incubated with CX4152 for 1 h and placed in the top wells of a chemotaxis plate containing 50 nM CXCL8 in the bottom wells. Neutrophils were allowed to migrate for 2–4 h at 37 °C and 5% CO$_2$. Inhibition of chemotaxis was evaluated on the basis of cell counts relative to the control (untreated with CXCL8). CX4152 concentration-dependently inhibited CXCL8-induced chemotaxis with an IC$_{50}$ value of 51.48 μM (95% confidence interval of 41.63 to 63.66 μM, r^2 = 0.92). Each data point is the mean ± SD of three experiments. (B) Attenuation of neutrophil recruitment in BALF of mice at 24 h by pretreatment with CX4152 prior to intranasal LPS challenge. CX4152 (50 mg/kg subcutaneously) significantly inhibited neutrophil influx (*, $p < 0.05$). Each value is the mean ± SD for three animals per treatment group ($N = 12$).
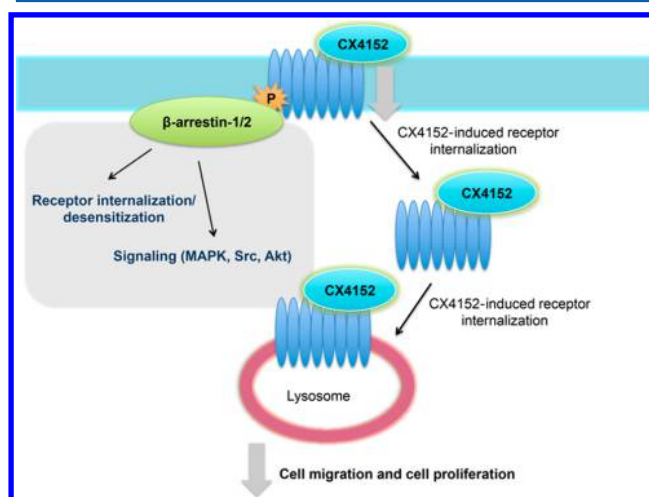

Figure 12. Schematic illustration of the proposed mechanism of action of CX4152. CX4152 induces receptor internalization in a time- and dose-dependent manner. CXCR2 internalization also leads to receptor degradation, perhaps via lysosomes, resulting in a reduction of the total CXCR2. This subsequently leads to decreased CXCR2/β-arrestin-2 association upon CXCL8 activation in the Tango assay. This is supported by data showing that the CX4152 inhibitory activity in the Tango assay is dependent on the pretreatment time.

chemokine receptors or other cellular targets. CX4152 induced receptor internalization within 10 min, suggesting that the inhibitory effects of CX4152 in the CXCR2 Tango assay are due to β-arrestin-2-independent receptor internalization. This phenomenon is most likely not due to receptor downregulation since the total CXCR2 expression was not decreased until 5 h later. Rather, at earlier time points the total CXCR2 appeared to increase, perhaps as a result of the accumulation of intracellular CXCR2. This is further supported by studies showing that CX4152 was more potent at inhibiting β-arrestin-2 recruitment in the CXCR2 Tango assay when cells were pretreated with CX4152 prior to CXCL8 stimulation than when cells were cotreated with CX4152

and CXCL8 at the same time (Figure 7C). These observations suggest that CX4152 may act as an agonist. However, it did not activate calcium mobilization (Figure 10). We postulate that CX4152 inhibits CXCR2/β-arrestin-2 association by down-regulating surface expression of CXCR2 (Figure 12). Through this mechanism, CX4152 inhibits CXCL8-mediated PMN cell migration and LPS-induced lung inflammation in mice (Figure 11). This mechanism of action has not been described in any previously reported CXCR2 antagonists to date.

■ ASSOCIATED CONTENT

Ⓢ Supporting Information

Supplementary materials and methods, suppplementary tables and figures, and a spreadsheet containing structures of compounds in the external validation database (XLSX). The Supporting Information is available free of charge on the ACS Publications website at DOI: 10.1021/acs.jcim.5b00181.

■ AUTHOR INFORMATION

Corresponding Author

*Phone: 734-647-2732. E-mail: neamati@umich.edu.

Author Contributions

‖T. Bensman and H. Ho contributed equally.

Notes

The authors declare no competing financial interest.

■ ACKNOWLEDGMENTS

■ ABBREVIATIONS USED

CXCR2, CXC receptor 2; CXCR1, CXC receptor 1; CXCR4, CXC receptor 4; CXCL8, interleukin-8; ENA-78, epithelial-cell-derived neutrophil-activating protein 78; NAP-2, neutrophil-activating peptide 2; ELR+, glutamate, leucine, arginine motif; COPD, chronic obstructive pulmonary disorder; CF, cystic fibrosis; GH, Güner–Henry; HBD, hydrogen-bond donor; HBA, hydrogen-bond acceptor; HY, hydrophobic; AR, aromatic ring; NEAA, nonessential amino acids; HEPES, 4-(2-hydroxyethyl)-piperazine-1-ethanesulfonic acid; TEV, tobacco etch virus; FRET, fluorescence resonance energy transfer; SDF-1, stromal-cell-derived factor 1; DMEM, Dulbecco's Modified Eagle's Medium; PBS, phosphate-buffered saline; FBS, fetal bovine serum; MTT, (3-(4,5-dimethylthiazol-2-yl)-2,5-diphenyltetrazolium bromide; RPMI, Roswell Park Memorial Institute; rpm, rotation per minute; EDTA, ethylenediaminetetraacetic acid; DMSO, dimethyl sulfoxide; BALF, bronchoalveolar lavage fluid; LPS, lipopolysaccharide; GOLD, Genetic Optimization for Ligand Docking; ROCS, Rapid Overlay of Chemical Structures

■ REFERENCES

(1) Baggiolini, M.; Dewald, B.; Moser, B. Interleukin-8 and Related Chemotactic Cytokines–CXC and CC Chemokines. *Adv. Immunol.* **1994**, *55*, 97–179.

(2) Xu, L.; Kelvin, D. J.; Ye, G. Q.; Taub, D. D.; Ben-Baruch, A.; Oppenheim, J. J.; Wang, J. M. Modulation of Il-8 Receptor Expression on Purified Human T Lymphocytes Is Associated with Changed Chemotactic Responses to Il-8. *J. Leukocyte Biol.* **1995**, *57*, 335–342.

(3) Chuntharapai, A.; Lee, J.; Hebert, C. A.; Kim, K. J. Monoclonal Antibodies Detect Different Distribution Patterns of Il-8 Receptor a and Il-8 Receptor B on Human Peripheral Blood Leukocytes. *J. Immunol.* **1994**, *153*, 5682–5688.

(4) Murdoch, C.; Monk, P. N.; Finn, A. CXC Chemokine Receptor Expression on Human Endothelial Cells. *Cytokine+* **1999**, *11*, 704–712.

(5) Horuk, R.; Martin, A. W.; Wang, Z.; Schweitzer, L.; Gerassimides, A.; Guo, H.; Lu, Z.; Hesselgesser, J.; Perez, H. D.; Kim, J.; Parker, J.; Hadley, T. J.; Peiper, S. C. Expression of Chemokine Receptors by Subsets of Neurons in the Central Nervous System. *J. Immunol.* **1997**, *158*, 2882–2890.

(6) Ahuja, S. K.; Murphy, P. M. The CXC Chemokines Growth-Regulated Oncogene (Gro) Alpha, Grobeta, Grogamma, Neutrophil-Activating Peptide-2, and Epithelial Cell-Derived Neutrophil-Activating Peptide-78 Are Potent Agonists for the Type B, but Not the Type a, Human Interleukin-8 Receptor. *J. Biol. Chem.* **1996**, *271*, 20545–20550.

(7) Murphy, P. M.; Tiffany, H. L. Cloning of Complementary DNA Encoding a Functional Human Interleukin-8 Receptor. *Science* **1991**, *253*, 1280–1283.

(8) Coffer, J. P.; Geijsen, N.; M'Rabet, L.; Schweizer, C. R.; Maikoe, T.; Raaijmakers, A. M. J.; Lammers, J.-W. J.; Koenderman, L. Comparison of the Roles of Mitogen-Activated Protein Kinase Kinase and Phosphatidylinositol 3-Kinase Signal Transduction in Neutrophil Effector Function. *Biochem. J.* **1998**, *329*, 121–130.

(9) Constantin, G.; Majeed, M.; Giagulli, C.; Piccio, L.; Kim, J. Y.; Butcher, E. C.; Laudanna, C. Chemokines Trigger Immediate Beta2 Integrin Affinity and Mobility Changes: Differential Regulation and Roles in Lymphocyte Arrest under Flow. *Immunity* **2000**, *13*, 759–769.

(10) Addison, C. L.; Daniel, T. O.; Burdick, M. D.; Liu, H.; Ehlert, J. E.; Xue, Y. Y.; Buechi, L.; Walz, A.; Richmond, A.; Strieter, R. M. The CXC Chemokine Receptor 2, CXCR2, Is the Putative Receptor for Elr+ CXC Chemokine-Induced Angiogenic Activity. *J. Immunol.* **2000**, *165*, 5269–5277.

(11) Nocker, R. E.; Schoonbrood, D. F.; van de Graaf, E. A.; Hack, C. E.; Lutter, R.; Jansen, H. M.; Out, T. A. Interleukin-8 in Airway Inflammation in Patients with Asthma and Chronic Obstructive Pulmonary Disease. *Int. Arch. Allergy Immunol.* **1996**, *109*, 183–191.

(12) Yamamoto, C.; Yoneda, T.; Yoshikawa, M.; Fu, A.; Tokuyama, T.; Tsukaguchi, K.; Narita, N. Airway Inflammation in Copd Assessed by Sputum Levels of Interleukin-8. *Chest* **1997**, *112*, 505–510.

(13) Busch-Petersen, J. Small Molecule Antagonists of the CXCR2 and CXCR1 Chemokine Receptors as Therapeutic Agents for the Treatment of Inflammatory Diseases. *Curr. Top. Med. Chem.* **2006**, *6*, 1345–1352.

(14) Widdowson, K. L. Phenyl Urea Interleukin-8 Receptor Antagonists for Treatment of Interleukin-8-Mediated Diseases, and Preparation Thereof. WO199749286, 1997.

(15) Zhu, Y. M.; Webster, S. J.; Flower, D.; Woll, P. J. Interleukin-8/CXCL8 Is a Growth Factor for Human Lung Cancer Cells. *Br. J. Cancer* **2004**, *91*, 1970–1976.

(16) Rubie, C.; Kollmar, O.; Frick, V. O.; Wagner, M.; Brittner, B.; Graber, S.; Schilling, M. K. Differential CXC Receptor Expression in Colorectal Carcinomas. *Scand. J. Immunol.* **2008**, *68*, 635–644.

(17) Murphy, C.; McGurk, M.; Pettigrew, J.; Santinelli, A.; Mazzucchelli, R.; Johnston, P. G.; Montironi, R.; Waugh, D. J. Nonapical and Cytoplasmic Expression of Interleukin-8, CXCR1, and CXCR2 Correlates with Cell Proliferation and Microvessel Density in Prostate Cancer. *Clin. Cancer Res.* **2005**, *11*, 4117–4127.

(18) Yang, G.; Rosen, D. G.; Liu, G.; Yang, F.; Guo, X.; Xiao, X.; Xue, F.; Mercado-Uribe, I.; Huang, J.; Lin, S. H.; Mills, G. B.; Liu, J. CXCR2 Promotes Ovarian Cancer Growth through Dysregulated Cell Cycle, Diminished Apoptosis, and Enhanced Angiogenesis. *Clin. Cancer Res.* **2010**, *16*, 3875–3886.

(19) Luppi, F.; Longo, A. M.; de Boer, W. I.; Rabe, K. F.; Hiemstra, P. S. Interleukin-8 Stimulates Cell Proliferation in Non-Small Cell Lung Cancer through Epidermal Growth Factor Receptor Transactivation. *Lung Cancer* **2007**, *56*, 25–33.

(20) Ning, Y.; Manegold, P. C.; Hong, Y. K.; Zhang, W.; Pohl, A.; Lurje, G.; Winder, T.; Yang, D.; LaBonte, M. J.; Wilson, P. M.; Ladner, R. D.; Lenz, H. J. Interleukin-8 Is Associated with Proliferation, Migration,

Angiogenesis and Chemosensitivity in Vitro and in Vivo in Colon Cancer Cell Line Models. *Int. J. Cancer* **2011**, *128*, 2038−2049.

(21) Waugh, D. J.; Wilson, C. The Interleukin-8 Pathway in Cancer. *Clin. Cancer Res.* **2008**, *14*, 6735−6741.

(22) Li, A.; Varney, M. L.; Singh, R. K. Constitutive Expression of Growth Regulated Oncogene (Gro) in Human Colon Carcinoma Cells with Different Metastatic Potential and Its Role in Regulating Their Metastatic Phenotype. *Clin. Exp. Metastasis* **2005**, *21*, 571−579.

(23) Ogata, H.; Sekikawa, A.; Yamagishi, H.; Ichikawa, K.; Tomita, S.; Imura, J.; Ito, Y.; Fujita, M.; Tsubaki, M.; Kato, H.; Fujimori, T.; Fukui, H. GRO*α* Promotes Invasion of Colorectal Cancer Cells. *Oncol. Rep.* **2010**, *24*, 1479−1486.

(24) Keane, M. P.; Belperio, J. A.; Xue, Y. Y.; Burdick, M. D.; Strieter, R. M. Depletion of CXCR2 Inhibits Tumor Growth and Angiogenesis in a Murine Model of Lung Cancer. *J. Immunol.* **2004**, *172*, 2853−2860.

(25) *Catalyst*, version 4.11; Accelrys, Inc.: San Diego, CA, 2005; http://www.accelrys.com.

(26) Jones, G.; Willett, P.; Glen, R. C.; Leach, A. R.; Taylor, R. Development and Validation of a Genetic Algorithm for Flexible Docking. *J. Mol. Biol.* **1997**, *267*, 727−748.

(27) Jones, G.; Willett, P.; Glen, R. C. Molecular Recognition of Receptor Sites Using a Genetic Algorithm with a Description of Desolvation. *J. Mol. Biol.* **1995**, *245*, 43−53.

(28) *ROCS*, version 3.2.0.4; OpenEye Scientific Software: Santa Fe, NM; http://www.eyesopen.com.

(29) Hawkins, P. C.; Skillman, A. G.; Nicholls, A. Comparison of Shape-Matching and Docking as Virtual Screening Tools. *J. Med. Chem.* **2007**, *50*, 74−82.

(30) Dwyer, M. P.; Yu, Y.; Chao, J.; Aki, C.; Chao, J.; Biju, P.; Girijavallabhan, V.; Rindgen, D.; Bond, R.; Mayer-Ezel, R.; Jakway, J.; Hipkin, R. W.; Fossetta, J.; Gonsiorek, W.; Bian, H.; Fan, X.; Terminelli, C.; Fine, J.; Lundell, D.; Merritt, J. R.; Rokosz, L. L.; Kaiser, B.; Li, G.; Wang, W.; Stauffer, T.; Ozgur, L.; Baldwin, J.; Taveras, A. G. Discovery of 2-Hydroxy-N,N-Dimethyl-3-{2-[[(R)-1-(5- Methylfuran-2-Yl)- Propyl]Amino]-3,4-Dioxocyclobut-1-Enylamino}Benzamide (Sch 527123): A Potent, Orally Bioavailable CXCR2/CXCR1 Receptor Antagonist. *J. Med. Chem.* **2006**, *49*, 7603−7606.

(31) Jin, Q.; Nie, H.; McCleland, B. W.; Widdowson, K. L.; Palovich, M. R.; Elliott, J. D.; Goodman, R. M.; Burman, M.; Sarau, H. M.; Ward, K. W.; Nord, M.; Orr, B. M.; Gorycki, P. D.; Busch-Petersen, J. Discovery of Potent and Orally Bioavailable N,N′-Diarylurea Antagonists for the CXCR2 Chemokine Receptor. *Bioorg. Med. Chem. Lett.* **2004**, *14*, 4375−4378.

(32) McCleland, B. W.; Davis, R. S.; Palovich, M. R.; Widdowson, K. L.; Werner, M. L.; Burman, M.; Foley, J. J.; Schmidt, D. B.; Sarau, H. M.; Rogers, M.; Salyers, K. L.; Gorycki, P. D.; Roethke, T. J.; Stelman, G. J.; Azzarano, L. M.; Ward, K. W.; Busch-Petersen, J. Comparison of N,N′-Diarylsquaramides and N,N′-Diarylureas as Antagonists of the CXCR2 Chemokine Receptor. *Bioorg. Med. Chem. Lett.* **2007**, *17*, 1713−1717.

(33) Merritt, J. R.; Rokosz, L. L.; Nelson, K. H., Jr.; Kaiser, B.; Wang, W.; Stauffer, T. M.; Ozgur, L. E.; Schilling, A.; Li, G.; Baldwin, J. J.; Taveras, A. G.; Dwyer, M. P.; Chao, J. Synthesis and Structure-Activity Relationships of 3,4-Diaminocyclobut-3-Ene-1,2-Dione CXCR2 Antagonists. *Bioorg. Med. Chem. Lett.* **2006**, *16*, 4107−4110.

(34) Nie, H.; Widdowson, K. L.; Palovich, M. R.; Fu, W.; Elliott, J. D.; Bryan, D. L.; Burman, M.; Schmidt, D. B.; Foley, J. J.; Sarau, H. M.; Busch-Petersen, J. N,N′-Diarylcyanoguanidines as Antagonists of the CXCR2 and CXCR1 Chemokine Receptors. *Bioorg. Med. Chem. Lett.* **2006**, *16*, 5513−5516.

(35) Widdowson, K. L.; Elliott, J. D.; Veber, D. F.; Nie, H.; Rutledge, M. C.; McCleland, B. W.; Xiang, J. N.; Jurewicz, A. J.; Hertzberg, R. P.; Foley, J. J.; Griswold, D. E.; Martin, L.; Lee, J. M.; White, J. R.; Sarau, H. M. Evaluation of Potent and Selective Small-Molecule Antagonists for the CXCR2 Chemokine Receptor. *J. Med. Chem.* **2004**, *47*, 1319−1321.

(36) *Discovery Studio 2.0*; Accelrys, Inc.: San Diego, CA, 2009; http://www.accelrys.com.

(37) Smellie, A.; Teig, S. L.; Towbin, P. Poling: Promoting Conformational Coverage. *J. Comput. Chem.* **1995**, *16*, 171−187.

(38) Smellie, A.; Kahn, S. D.; Teig, S. L. Analysis of Conformational Coverage. 1. Validation and Estimation of Coverage. *J. Chem. Inf. Model.* **1995**, *35*, 285−294.

(39) Smellie, A.; Kahn, S. D.; Teig, S. L. Analysis of Conformational Coverage. 2. Applications of Conformational Models. *J. Chem. Inf. Model.* **1995**, *35*, 295−304.

(40) Güner, O. F.; Henry, D. R. Metric for Analyzing Hit Lists and Pharmacophores. In *Pharmacophore Perception, Development, and Use in Drug Design*; Güner, O. F., Ed.; International University Line: La Jolla, CA, 2000; Chapter 11, pp 193−212.

(41) Aki, C.; Chao, J.; Ferreira, J. A.; Dwyer, M. P.; Yu, Y.; Chao, J.; Merritt, R. J.; Lai, G.; Wu, M.; Hipkin, R. W.; Fan, X.; Gonsiorek, W.; Fosseta, J.; Rindgen, D.; Fine, J.; Lundell, D.; Taveras, A. G.; Biju, P. Diaminocyclobutenediones as Potent and Orally Bioavailable CXCR2 Receptor Antagonists: Sar in the Phenolic Amide Region. *Bioorg. Med. Chem. Lett.* **2009**, *19*, 4446−4449.

(42) Biju, P.; Taveras, A. G.; Dwyer, M. P.; Yu, Y.; Chao, J.; Hipkin, R. W.; Fan, X.; Rindgen, D.; Fine, J.; Lundell, D. Fluoroalkyl Alpha Side Chain Containing 3,4-Diamino-Cyclobutenediones as Potent and Orally Bioavailable CXCR2-CXCR1 Dual Antagonists. *Bioorg. Med. Chem. Lett.* **2009**, *19*, 1431−1433.

(43) Chao, J.; Taveras, A. G.; Chao, J.; Aki, C.; Dwyer, M.; Yu, Y.; Purakkattle, B.; Rindgen, D.; Jakway, J.; Hipkin, W.; Fosetta, J.; Fan, X.; Lundell, D.; Fine, J.; Minnicozzi, M.; Phillips, J.; Merritt, J. R. C(4)-Alkyl Substituted Furanyl Cyclobutenediones as Potent, Orally Bioavailable CXCR2 and CXCR1 Receptor Antagonists. *Bioorg. Med. Chem. Lett.* **2007**, *17*, 3778−3783.

(44) Baxter, A.; Bennion, C.; Bent, J.; Boden, K.; Brough, S.; Cooper, A.; Kinchin, E.; Kindon, N.; McInally, T.; Mortimore, M.; Roberts, B.; Unitt, J. Hit-to-Lead Studies: The Discovery of Potent, Orally Bioavailable Triazolethiol CXCR2 Receptor Antagonists. *Bioorg. Med. Chem. Lett.* **2003**, *13*, 2625−2628.

(45) Hunt, F.; Austin, C.; Austin, R.; Bonnert, R.; Cage, P.; Christie, J.; Christie, M.; Dixon, C.; Hill, S.; Jewell, R.; Martin, I.; Robinson, D.; Willis, P. Sar Studies on Thiazolo[4,5-D]Pyrimidine Based CXCR2 Antagonists Involving a Novel Tandem Displacement Reaction. *Bioorg. Med. Chem. Lett.* **2007**, *17*, 2731−2734.

(46) Porter, D. W.; Bradley, M.; Brown, Z.; Canova, R.; Charlton, S.; Cox, B.; Hunt, P.; Kolarik, D.; Lewis, S.; O'Connor, D.; Reilly, J.; Spanka, C.; Tedaldi, L.; Watson, S. J.; Wermuth, R.; Press, N. J. The Discovery of Potent, Orally Bioavailable Pyrazolo and Triazolopyrimidine CXCR2 Receptor Antagonists. *Bioorg. Med. Chem. Lett.* **2014**, *24*, 72−76.

(47) Walters, I.; Austin, C.; Austin, R.; Bonnert, R.; Cage, P.; Christie, M.; Ebden, M.; Gardiner, S.; Grahames, C.; Hill, S.; Hunt, F.; Jewell, R.; Lewis, S.; Martin, I.; Nicholls, D.; Robinson, D. Evaluation of a Series of Bicyclic CXCR2 Antagonists. *Bioorg. Med. Chem. Lett.* **2008**, *18*, 798−803.

(48) Wang, Y.; Busch-Petersen, J.; Wang, F.; Ma, L.; Fu, W.; Kerns, J. K.; Jin, J.; Palovich, M. R.; Shen, J. K.; Burman, M.; Foley, J. J.; Schmidt, D. B.; Hunsberger, G. E.; Sarau, H. M.; Widdowson, K. L. 3-Arylamino-2h-1,2,4-Benzothiadiazin-5-Ol 1,1-Dioxides as Novel and Selective CXCR2 Antagonists. *Bioorg. Med. Chem. Lett.* **2007**, *17*, 3864−3867.

(49) Winters, M. P.; Crysler, C.; Subasinghe, N.; Ryan, D.; Leong, L.; Zhao, S.; Donatelli, R.; Yurkow, E.; Mazzulla, M.; Boczon, L.; Manthey, C. L.; Molloy, C.; Raymond, H.; Murray, L.; McAlonan, L.; Tomczuk, B. Carboxylic Acid Bioisosteres Acylsulfonamides, Acylsulfamides, and Sulfonylureas as Novel Antagonists of the CXCR2 Receptor. *Bioorg. Med. Chem. Lett.* **2008**, *18*, 1926−1930.

(50) Yu, Y.; Dwyer, M. P.; Chao, J.; Aki, C.; Chao, J.; Purakkattle, B.; Rindgen, D.; Bond, R.; Mayer-Ezel, R.; Jakway, J.; Qiu, H.; Hipkin, R. W.; Fossetta, J.; Gonsiorek, W.; Bian, H.; Fan, X.; Terminelli, C.; Fine, J.; Lundell, D.; Merritt, J. R.; He, Z.; Lai, G.; Wu, M.; Taveras, A. Synthesis and Structure-Activity Relationships of Heteroaryl Substituted-3,4-Diamino-3-Cyclobut-3-Ene-1,2-Dione CXCR2/CXCR1 Receptor Antagonists. *Bioorg. Med. Chem. Lett.* **2008**, *18*, 1318−1322.

(51) Cutshall, N. S.; Ursino, R.; Kucera, K. A.; Latham, J.; Ihle, N. C. Nicotinamide N-Oxides as CXCR2 Antagonists. *Bioorg. Med. Chem. Lett.* **2001**, *11*, 1951−1954.

(52) Liu, S.; Liu, Y.; Wang, H.; Ding, Y.; Wu, H.; Dong, J.; Wong, A.; Chen, S. H.; Li, G.; Chan, M.; Sawyer, N.; Gervais, F. G.; Henault, M.; Kargman, S.; Bedard, L. L.; Han, Y.; Friesen, R.; Lobell, R. B.; Stout, D. M. Design, Synthesis, and Evaluation of Novel 3-Amino-4-Hydrazine-Cyclobut-3-Ene-1,2-Diones as Potent and Selective CXCR2 Chemokine Receptor Antagonists. *Bioorg. Med. Chem. Lett.* **2009**, *19*, 5741−5745.

(53) Lu, H.; Yang, T.; Xu, Z.; Wren, P. B.; Zhang, Y.; Cai, X.; Patel, M.; Dong, K.; Zhang, Q.; Zhang, W.; Guan, X.; Xiang, J.; Elliott, J. D.; Lin, X.; Ren, F. 2-Aminopyrimidin-4(1h)-One as the Novel Bioisostere of Urea: Discovery of Novel and Potent CXCR2 Antagonists. *Bioorg. Med. Chem. Lett.* **2014**, *24*, 5493−5496.

(54) Maeda, D. Y.; Peck, A. M.; Schuler, A. D.; Quinn, M. T.; Kirpotina, L. N.; Wicomb, W. N.; Fan, G. H.; Zebala, J. A. Discovery of 2-[5-(4-Fluorophenylcarbamoyl)Pyridin-2-Ylsulfanylmethyl]Phenylboronic Acid (Sx-517): Noncompetitive Boronic Acid Antagonist of CXCR1 and CXCR2. *J. Med. Chem.* **2014**, *57*, 8378−8397.

(55) Porter, D. W.; Bradley, M.; Brown, Z.; Charlton, S. J.; Cox, B.; Hunt, P.; Janus, D.; Lewis, S.; Oakley, P.; O'Connor, D.; Reilly, J.; Smith, N.; Press, N. J. The Discovery of Potent, Orally Bioavailable Pyrimidine-5-Carbonitrile-6-Alkyl CXCR2 Receptor Antagonists. *Bioorg. Med. Chem. Lett.* **2014**, *24*, 3285−3290.

(56) Isberg, V.; Vroling, B.; van der Kant, R.; Li, K.; Vriend, G.; Gloriam, D. Gpcrdb: An Information System for G Protein-Coupled Receptors. *Nucleic Acids Res.* **2014**, *42*, D422−425.

(57) Fiser, A.; Sali, A. Modloop: Automated Modeling of Loops in Protein Structures. *Bioinformatics* **2003**, *19*, 2500−2501.

(58) Hawkins, P. C.; Skillman, A. G.; Warren, G. L.; Ellingson, B. A.; Stahl, M. T. Conformer Generation with Omega: Algorithm and Validation Using High Quality Structures from the Protein Databank and Cambridge Structural Database. *J. Chem. Inf. Model.* **2010**, *50*, 572−584.

(59) Altenburg, J. D.; Broxmeyer, H. E.; Jin, Q.; Cooper, S.; Basu, S.; Alkhatib, G. A Naturally Occurring Splice Variant of Cxcl12/Stromal Cell-Derived Factor 1 Is a Potent Human Immunodeficiency Virus Type 1 Inhibitor with Weak Chemotaxis and Cell Survival Activities. *J. Virol.* **2007**, *81*, 8140−8148.

(60) Carmichael, J.; DeGraff, W. G.; Gazdar, A. F.; Minna, J. D.; Mitchell, J. B. Evaluation of a Tetrazolium-Based Semiautomated Colorimetric Assay: Assessment of Chemosensitivity Testing. *Cancer Res.* **1987**, *47*, 936−942.

(61) Kilkenny, C.; Browne, W. J.; Cuthill, I. C.; Emerson, M.; Altman, D. G. Improving Bioscience Research Reporting: The Arrive Guidelines for Reporting Animal Research. *PLoS Biol.* **2010**, *8*, e1000412.

(62) McGrath, J. C.; Drummond, G. B.; McLachlan, E. M.; Kilkenny, C.; Wainwright, C. L. Guidelines for Reporting Experiments Involving Animals: The Arrive Guidelines. *Br. J. Pharmacol.* **2010**, *160*, 1573−1576.

(63) Dayam, R.; Aiello, F.; Deng, J.; Wu, Y.; Garofalo, A.; Chen, X.; Neamati, N. Discovery of Small Molecule Integrin Alphavbeta3 Antagonists as Novel Anticancer Agents. *J. Med. Chem.* **2006**, *49*, 4526−4534.

(64) *Pharmacophore Perception, Development, and Use in Drug Design*; Güner, O. F., Ed.; International University Line: La Jolla, CA, 2000.

(65) Vitas-M Laboratory Screening Compounds. www.vitasmlab.com.

(66) Enamine Screening Collection. http://www.enamine.net/.

(67) Asinex Libraries. www.asinex.com.

(68) de Kruijf, P.; van Heteren, J.; Lim, H. D.; Conti, P. G. M.; van der Lee, M. M. C.; Bosch, L.; Ho, K.-K.; Auld, D.; Ohlmeyer, M.; Smit, M. J.; Wijkmans, J. C. H. M.; Zaman, G. J. R.; Smit, M. J.; Leurs, R. Nonpeptidergic Allosteric Antagonists Differentially Bind to the CXCR2 Chemokine Receptor. *J. Pharmacol. Exp. Ther.* **2009**, *329*, 783−790.

(69) Salchow, K.; Bond, M. E.; Evans, S. C.; Press, N. J.; Charlton, S. J.; Hunt, P. A.; Bradley, M. E. A Common Intracellular Allosteric Binding Site for Antagonists of the CXCR2 Receptor. *Br. J. Pharmacol.* **2010**, *159*, 1429−1439.

(70) Singh, S.; Sadanandam, A.; Varney, M. L.; Nannuru, K. C.; Singh, R. K. Small Interfering Rna-Mediated CXCR1 or CXCR2 Knock-Down Inhibits Melanoma Tumor Growth and Invasion. *Int. J. Cancer* **2010**, *126*, 328−336.

(71) Goda, A. E.; Koyama, M.; Sowa, Y.; Elokely, K. M.; Yoshida, T.; Kim, B. Y.; Sakai, T. Molecular Mechanisms of the Antitumor Activity of Sb225002: A Novel Microtubule Inhibitor. *Biochem. Pharmacol.* **2013**, *85*, 1741−1752.

(72) Du, M.; Qiu, Q.; Gruslin, A.; Gordon, J.; He, M.; Chan, C. C.; Li, D.; Tsang, B. K. Sb225002 Promotes Mitotic Catastrophe in Chemo-Sensitive and -Resistant Ovarian Cancer Cells Independent of P53 Status in Vitro. *PLoS One* **2013**, *8*, e54572.

(73) Palm, K.; Luthman, K.; Ungell, A. L.; Strandlund, G.; Artursson, P. Correlation of Drug Absorption with Molecular Surface Properties. *J. Pharm. Sci.* **1996**, *85*, 32−39.

(74) Jiang, S.; Chow, S. C.; Nicotera, P.; Orrenius, S. Intracellular Ca^{2+} Signals Activate Apoptosis in Thymocytes: Studies Using the Ca^{2+}-ATPase Inhibitor Thapsigargin. *Exp. Cell Res.* **1994**, *212*, 84−92.